Graphical Abstract

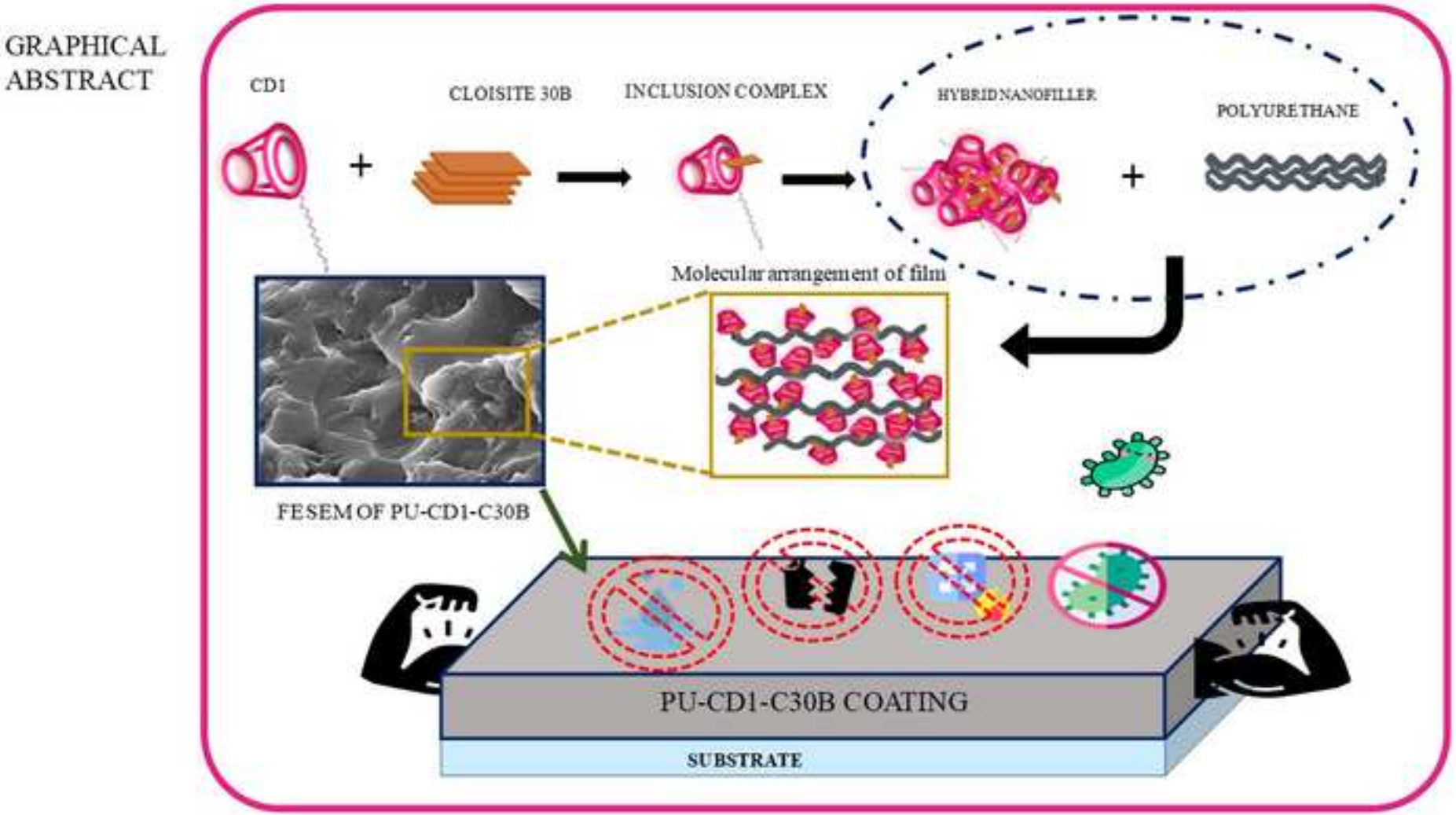

Highlights:

- Synthesis of sulfonated β- cyclodextrin (CD1) and its inclusion complex with nanocurcumin & Cloisite 30B clay.
- CD1 and hybrid nanofillers incorporated in the polyurethane (PU) matrix for anti-bacterial characteristics.
- Enhancement in heat resistance by more than 60% and ultimate tensile strength improved by more than 15%.
- Host-guest incorporation of the CD1 has exhibited hybrid nanofiller that have the chemical, philic, thermal and mechanical resistance.
- Callister model, mathematical model has been modified and applied to experimental results.

Sulfonated β-cyclodextrin-nanocurcumin/clay hybrid multi-functional polyurethane coatings

Anjali Sharma[a], Indu Pal Kaur[e], Fengge Gao[d],Gaurav Verma[a,b,c*]

[a]Dr. Shanti Swarup Bhatnagar University Institute of Chemical Engineering and Technology (formerlyDepartment of Chemical Engineering & Technology), Panjab University, Chandigarh-160014, India
[b]Centre for Nanoscience & Nanotechnology, University Institute for Emerging Areas in Science andTechnology, Panjab University, Chandigarh-160014, India.
[c]Energy Research Centre, Panjab University, Chandigarh-160014, India
[d]School of Science and Technology Nottingham Trent University, Clifton Lane, Nottingham, NG11 8NS, United Kingdom.
[e]University Institute of Pharmaceutical Sciences,Panjab University, Chandigarh- 160014
Corresponding Author: gauravvermas@gmail.com, gauravverma@pu.ac.in

Abstract:

Sulfonated β – cyclodextrin (CD1) exhibits anti-bacterial feature properties ascribed to its amphiphilic structure having hydrophobic cavity. To achieve a multifunctional surface coating an inclusion complex has been synthesized. This inclusion complex is achieved via co-precipitation method by amalgamating CD1 with Cloisite 30B (C30B) and nanocurcumin separately. Later this is imbibed as hybrid nanofiller into polyurethane (PU) coatings via in-situ polymerization. Host-guest, hydrophobic, van der Waal (hydrogen bonding) and alkene reduction combine into supramolecular interactions in the nanocomposite coatings. The integration of amphiphilic CD1 with nanocurcumin solid-lipid nanoparticles (NC) and C30B reduced its hydrophilic interactions hence creating resistance to water molecules. The nanocomposite coating samples exhibit 60% increases in heat resistance and 78% enhancement in toughness and resistance to bacterial growth. A modified mathematical model has been applied to quantify the correlation between theoretical and experimental analysis.

Key words: Sulfonated β-cyclodextrin; hybrid nanofiller; polyurethane coating; anti-bacterial; inclusion complex; host-guest interactions

INTRODUCTION

Polyurethane (PU) coating finds application in every area of material engineering, from a pin to aeronautics because of its multifaceted properties. PU can be as robust as metals while being soft and elastic as rubbers, thus substituting different metals, plastics, and rubber-based

applications[1–6]. PU plays a vital role in medical science and is multifaceted, right from the construction materials used to build wards to beddings, surgical instruments, medical implants and ultimately micro scale encapsulation devices[7–10]. Recent experience with Covid19 forces us to reassess the structural devices which come into direct or indirect contact with the patients. Essential attributes for this purpose are biocompatibility along with flexibility, tensile strength, and of course process-ability[11,12]. There is a restricted range of synthetic organic polymers conforming to medical applications[13,14]. PU due to its varied chemistry of diisocyanate and diol monomers, can be altered to provide materials with wide–rangingproperties, such as melting or softening point and mechanical strength[14–18]. PU's key advantages have been its durability, hardness, and good chemical resistance. In biomedical applications, biomaterial-associated infection (BAI) is a major challenge that prevents smooth usage of polymeric materials[19,20]. Medical implant failure and subsequent patient mortality results from the adhesion and growth of harmful bacteria on implant materials and devices[13,14,16,20–22]. Filled or surface coated materials may be able to provide solutions to this issue. For this purpose unique fillers and nanohybrid need to be constructed.

Cyclodextrin are available in a variety of forms based on the quantity of glucose units. Three of the most significant cyclodextrins are α-, β-, and γ-CDs, which have 6, 7, and 8 glucose units, respectively[24–26]. Among them, β-CD garners the most attention because of easy production method and great output. As a carrier of an antibacterial agent or medicine, β-CD and its derivatives are among the most effective materials[7,25,27,28]. The in-vitro antibacterial activity of cyclodextrin-drug complexes including cyclodextrin and its derivatives are investigated. It is a broad-spectrum antibacterial medication to which most gram-negative bacteria and gram-positive bacteria are sensitive[29–31]. Cyclodextrin has direct applications in controlling infections in hospitals and has been integrated in the PUmatrix; also its incorporation has been done with the various other fillers such as nanocurcumin and organoclay (C30B). Attachment of nanocurcumin has been done to sulfonated β-cyclodextrin to enhance the anti-microbial activity. Similarly the C30B has been attached to the sulfonated β-cyclodextrin to reduce its chemical, thermal and mechanical degradation.

MATERIALS AND METHOD

PU monomers (Desmophen 680 BA (branched hydroxyl bearing polyester)) and Desmodur N3390 BA/SN (an aliphatic polyisocyanate-HDI biuret) are gratis by Covestro India Pvt. Ltd. Mumbai. 11-bromo-1-undecene, sodium sulfite (Na_2SO_3), methanol (MeOH) 2, 2-dimethoxy-2-phenylacetophenone, dimethyl sulfoxide (DMSO), ethanol (EtOH) have been purchased from Sigma-Aldrich chemical Pvt. Ltd., Bangalore. Heptakis-(6-deoxy-6-mercapto) - β-CD has been imported from Cyclodextrin-Shop, Netherlands. Organoclay Cloisite 30B (C30B) is supplied from Southern Clay Products, Inc. Texas, USA. A Nanocurcumin solid-lipid nanoparticle (NC) (batch no. 240820211PKCmn) is provided by the IPK laboratory (UIPS), Panjab University. Organic solvent acetone has been purchased from Fisher Scientific Pvt. Ltd., Mumbai. The catalyst used to cure nanocomposite coating is dibutyltin (IV) dilaurate (DBTL) has been gratis by Covestro India Pvt. Ltd. Mumbai.

1) Synthesis sodiumundec-10-ene-1-sulfonate crystals and Sulfonated β – Cyclodextrin (CD1):

- 2.122 gm of 11-bromo-1-undecene and 3.061 gm of sodium sulfite is added into a mixture of methanol/water (25/45 ml) and refluxed for 18 hours. Methanol has been removed and washed the aqueous layer with ethanol then dried. Hot methanol is used to extract white crystals after filtration. Ethanol/water mixture is used to recrystallize the crystals of sodiumundec-10-ene-1-sulfonate.
- 50mg of Heptakis-(6-deoxy-6-mercapto) - β-CD, 108mg of sodiumundec-10-ene-1-sulfonate and 22mg of 2,2-dimethoxy-2-phenylacetophenone in 5ml of DMSO. The reaction mixture is placed under an ultraviolet (UV) radiation (250 W) for 18 hours with continuous stirring. Product is precipitated by the addition of ethanol and collected by centrifugation, washed and collected.

2) Synthesis of (host) sulfonated β – cyclodextrin (CD1) – (guest) NC/organoclay (C30B) via Co-precipitation method.

- 0.5 mg of guest and host is swelled in 10 mL of acetone, followed by ultrasonication for 2 hrs.Next, 1:1 ratio of host and guest ultrasonicated suspension in acetone are placed in a beaker, followed by ultrasonication for 30 min. Subsequently, 40.0 μL of ammonia solution is injected into the mixture. After vigorous stirring for 3 min at room temperature, the inclusion complex (nanohybrid) suspension is collected.
- Synthesis of uncured suspension and coatings using in-situ polymerization:

Hybrid nanofillers have been swelled in the acetone solvent using ultrasonication bath (U). Desmophen is added to the swelled slurry using a simultaneous sequence of ultrasonication bath and high shear homogenizer (H).To cure the sample for coatings, Desmodur is added in the ratio of 3:1 to the uncured slurry using mechanical mixing at 4000 rpm with few drops of DBDTL catalyst and the spin coating has beenused for sample preparation.

CHARACTERIZATION:

The produced materials' X-ray diffraction (XRD) patterns have been analyzed using a Philips X'pert PRO240 mm diffractometer. It is equipped with an integrated germanium detector Cu-Ka, radiation source λ= 1.54060 Å working at 45KV and 40mA. The equatorial scans have been collected in continuous mode from 3.7° to 40° at a step of 0.017° with a scan step time of 24.4 seconds. Structural characterization is accomplished by FTIR spectrum by Perkin-Elmer spectrum RX-IFTIR in the 500-4000 cm-1 range. To investigate the elemental distribution in the hybrid nanofiller dispersed solution, energy-dispersive spectroscopy (EDS) has been used along mapping analysis, to create elemental maps on the nanoscale. Field emission scanning electron microscopy (FESEM; Hitachi, Japan, SU8000 Series) at an accelerating voltage of 5.0 kV has been used to investigate the nanocomposite coatings. Water contact angle was examined by Kruss DSA-100 at 29±5 °C. Water and THF immersion test have been conducted according to ASTMD 570 standard. To evaluate the thermal degradation TGA and DSC scans have generated by SDT650 simultaneous thermal analyzer by TA instruments and flame retardance has been conducted based on ASTM D 635 standard.To evaluate mechanical properties tensile testing has been performed on BISS UTM 400N, at ASTM D638 standard.

Well diffusion test has been performed for anti-bacterial activity; the zone of inhibition studies has been performed to measure the relative level of anti-microbial activity of control and the prepared coatings. The sterile agar plates have been cultured with gram-positive, gram-negative bacteria such as Escherichia coli (*E.coli*) (0157:H7), Staphylococcus aureus (*S.aureus*) (ATCC 9144) respectively according to ATCC protocols/ specifications. The bacterial cultures are harvested from the inoculated cultures in nutrient broth left to grow 12 hours at 37°C and harvest in the mid-exponential growth phase to obtain a final concentration of 105 colony forming units CFU/mL followed by centrifugation. The obtained palette of cells needs to be washed three times and re-suspended in PBS to remove residual

macromolecules and other constituents. Then, growth of selected microbes will be monitored spectrophotometrically by measuring the absorption at 600 nm. Cell suspension is diluted up to the desired concentration of 105 colony forming units CFU/mL to bring the desired initial optical density. After obtaining the pure cultures of microbes, Nutrient agar plates are to be made for zone of inhibition studies. The agar plates are inoculated with the standardized inoculums of the test microorganism. Then, the test compound at a desired concentration is placed in the agar well. Petri dishes are incubated under suitable conditions of 37°C for 24 hrs. Generally, anti-microbial agents diffuse into the agar and inhibit the germination and growth of the test microorganisms then measured the diameter of inhibition growth zones.

Theoretical approach:

Callister model [32] proposed a simple relation for the interfacial interaction of polymer composites on the basis of the study of relative yield strength;

$$\sigma_R = 1 - \left(1 - \frac{\alpha S}{\sigma_m}\right)\varphi \qquad (1)$$

Where "σ_R"is relative yield strength as $\sigma_R = \sigma_c/\sigma_m$;σc and σm are the yield strengths of the composite and the polymer matrix, respectively. "α" is the aspect ratio of the filler."S" is an interfacial stress transfer parameter, which shows the quality of interfacial adhesion at the interface and"φ" is the volume fraction of the filler.

Modified Callister model for thermal analysis

$$T_R = 1 - \left(1 - \frac{\alpha S}{\sigma_m}\right)\varphi \qquad (2)$$

Where T_R is soft segment derivative temperature defined as $T_R = Tc/Tm$; where T_c and T_m are composite and the polymer matrix soft segment derivative temperature. "S" stress transfer parameter defines the interfacial strength of material and "α" is the aspect ratio of filler.

RESULTS AND DISCUSSION:

Fig.1a represents the FT-IR spectrum of Na_2SO_3, sodiumundec-10-ene-1-sulfonate and CD1 from 4000 to 500 cm^{-1}. In Na_2SO_3 spectra, a band with overlapped three different transmittance peaks at 3547.94 cm^{-1}, 3472.69 cm^{-1}, and 3415.38 cm^{-1} referring to the hydroxyl group, H-bonded OH stretch (internally bonded OH stretch), and intermolecular O-H stretching respectively (table 1)[33]. These peaks are merged and broadened in sodiumundec-10-ene-1-sulfonate spectra. Also, thetwo new peaks have appeared at 2925.28 cm^{-1} and 975 cm^{-1}, inferring the asymmetric /symmetric stretching of CH_2 (methylene) and C=C bending respectively[34]. These peaks are evidentin the synthesis of sodiumundec-10-

ene-1-sulfonate, reaction scheme of 11-bromo-1-undecene attached to sodium sulfite are displayed at fig.1b. Additionally, the disappearance of these peaks in CD1 and the appearance of a new peak at 637 cm^{-1}(demonstrates C-S stretching) [35] confirms the synthesis of CD1. The existence of heptakis-(6-deoxy-6-mercapto)-β-CD is assured by the C-O-C stretching at 1115 cm^{-1} and the absorption band at 1735.39 cm^{-1} signifying six membered ring ketone or esters[35]. The attachment of heptakis-(6-deoxy-6-mercapto)-β-CD to sodium undec-10-ene-1-sulfonate fabricated CD1 is used as filler for PU antibacterial surface coating.

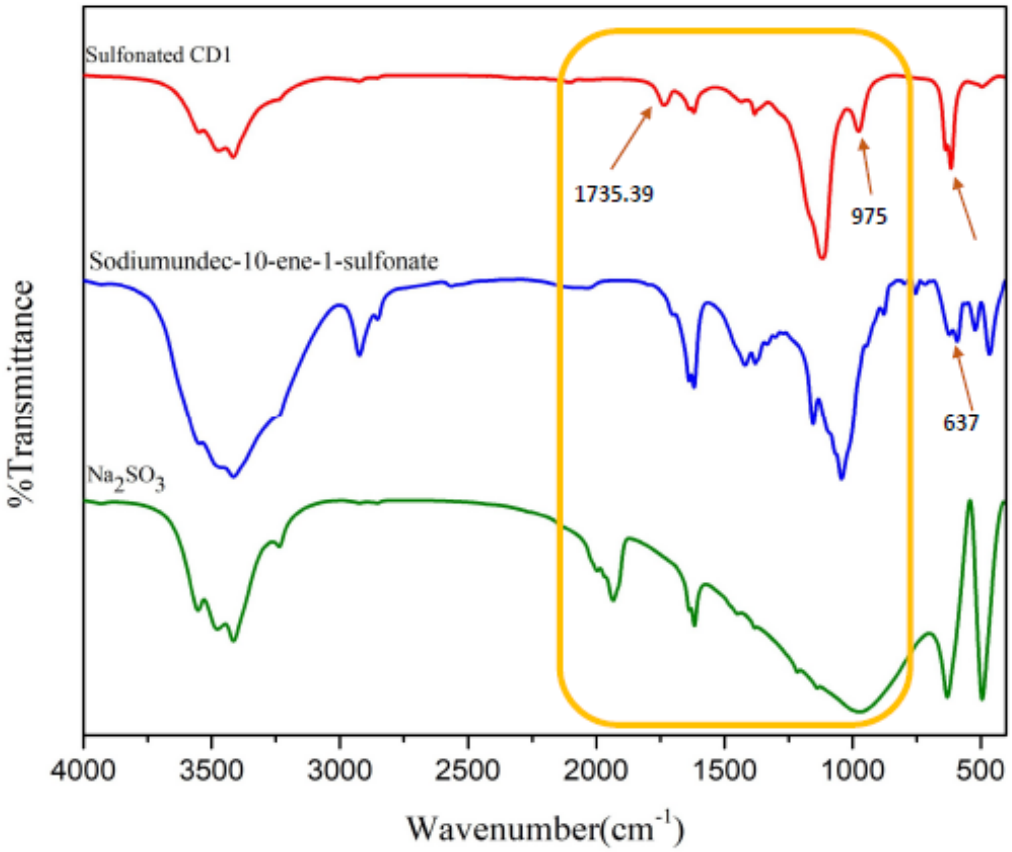

Fig.1. shows the FTIR spectra of Na_2SO_3, sodiumundec-10-ene-1-sulfonate and CD1

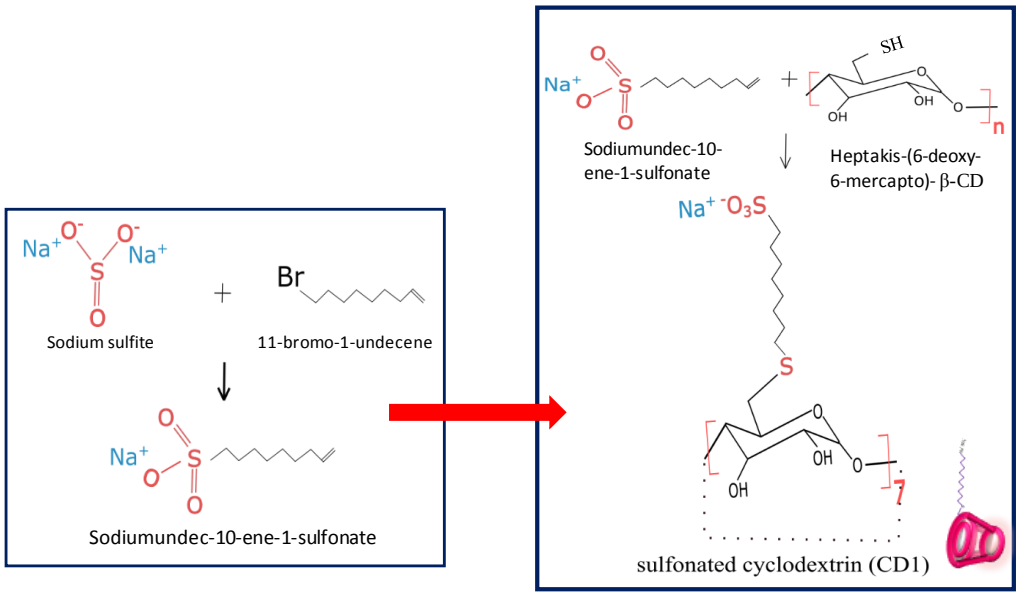

Fig.2. shows the reaction scheme of sodiumundec-10-ene-1-sulfonate and CD1.

Fig.4d.displays the broad peak at 3459 cm^{-1} corresponds to the overlapping of N-H, phenolic and alcoholic OH stretching vibration caused by the presence of CD1 and PU[34,36]. Hydrophobic interactions between the host and guest as well as non-covalent bonding forces such as hydrogen bonding and van der Waal forces are the main driving forces in the synthesis of inclusion complex of CD1 with NC and C30B[27,37].The IR spectra of PU-CD1 have absorption peak at 1051cm^{-1} confirming the C-C, C-O and C-O-C of saccharides stretching in PU matrix. In PU-CD1 graph 1638 cm^{-1} and 1618cm^{-1}H-bonded C=O, it evident the hydrogen bonding of CD1 with PU (fig.4f). Also, the absorption peak 1681cm-1 ((C=O) free) have high intensity than 1721 cm^{-1} ((C=O) bonded) which confirms the H-bonded C=O in PU-CD1-NC and PU-CD1-C30B[38,39] (fig.4).

Table 1: FTIR peaks description of Na_2SO_3, sodiumundec-10-ene-1-sulfonate and CD1.

Peaks (cm^{-1})	Functional Groups
3547.94	Hydroxyl group , H bonded OH stretch or Dimeric OH stretch or internally bonded OH stretch
3472.69	Dimeric OH stretch
3415.38	NH stretch (Aromatic primary amine) or O-H stretching intermolecular bonded
2925.28	Methylene CH asym/sym stretching
2106.11	cyanide, thiocyanate ion and related ions
1735.39	Six membered ring ketone or esters

1638	C=O (H-bonded)
1618	C=O (H-bonded)
1681	C=O (free)
1433	Methyl bonding
1381	Phenol or tertiary alcohol, OH bend or gem- Dimethyl or ‘iso’
1116	C-O-C stretching
975	C=C Bending
637	CH_3 -S- (C-S stretch) (C-S Mercaptans)

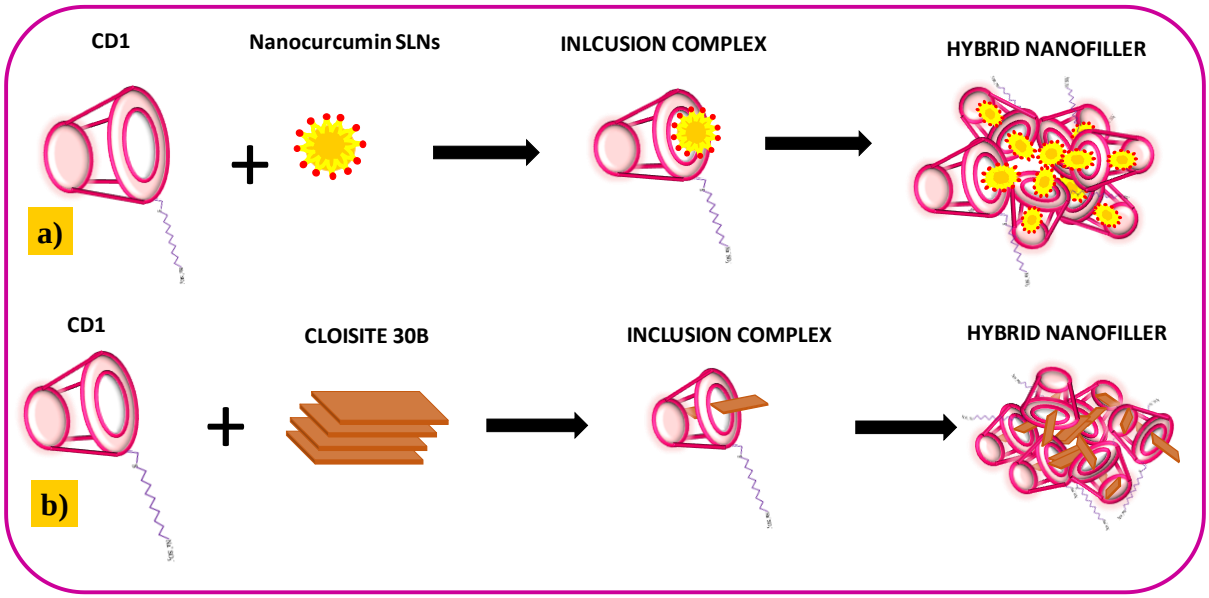

Fig.3. Schematic reaction illustration of inclusion complex of CD1 and nanofillers a) CD1-nanocurucmin SLNs (CD1-NC) and b) CD1-Cloisite 30B (CD1-C30B)

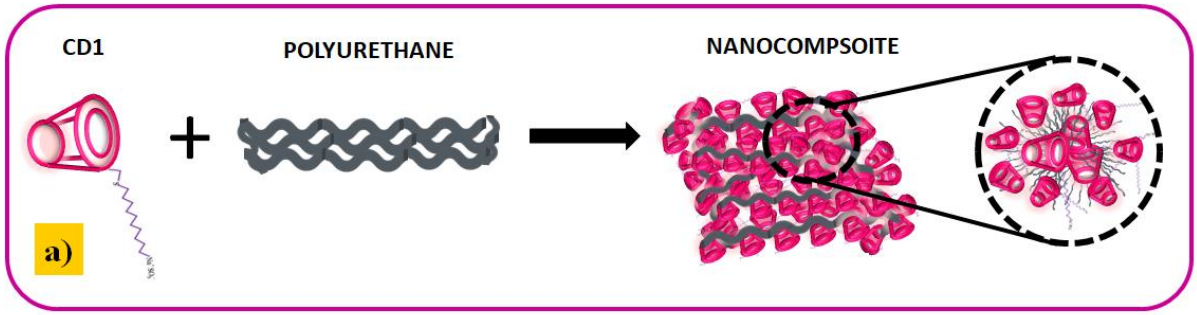

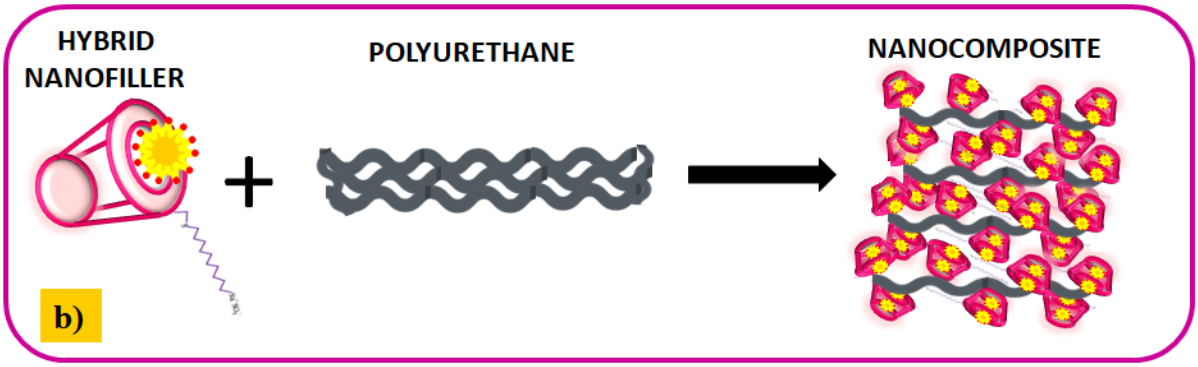
HYBRID
NANOFILLER
POLYURETHANE
NANOCOMPOSITE
b)

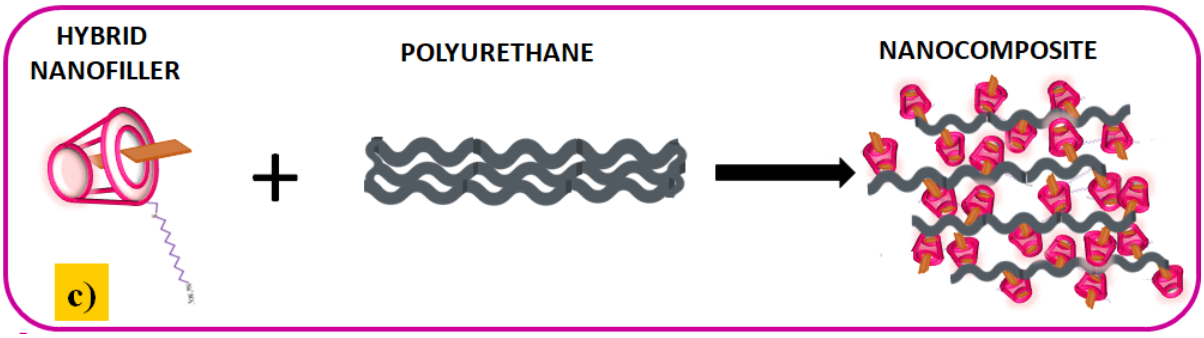
HYBRID
NANOFILLER
POLYURETHANE
NANOCOMPOSITE
c)

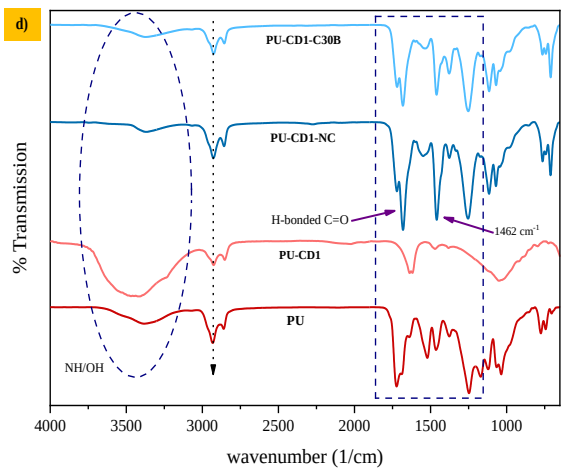
d)
PU-CD1-C30B
PU-CD1-NC
H-bonded C=O
1462 cm-1
PU-CD1
PU
NH/OH
% Transmission
4000
3500
3000
2500
2000
1500
1000
wavenumber (1/cm)

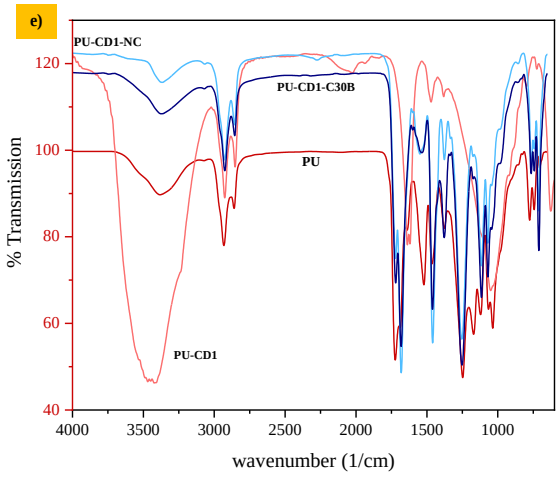
e)
PU-CD1-NC
PU-CD1-C30B
PU
PU-CD1
% Transmission
120
100
80
60
40
4000
3500
3000
2500
2000
1500
1000
wavenumber (1/cm)

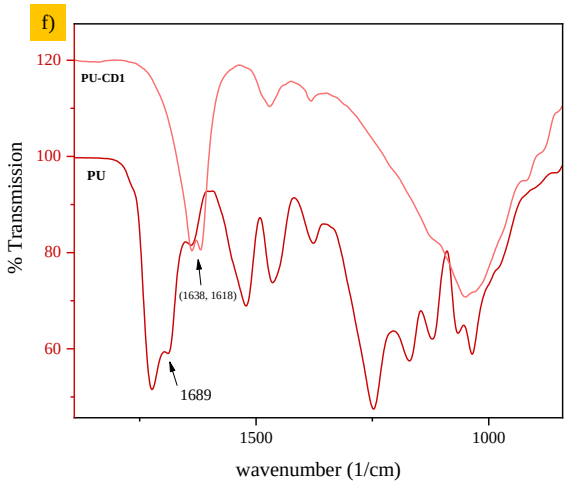
f)
PU-CD1
PU
(1638, 1618)
1689
% Transmission
120
100
80
60
1500
1000
wavenumber (1/cm)

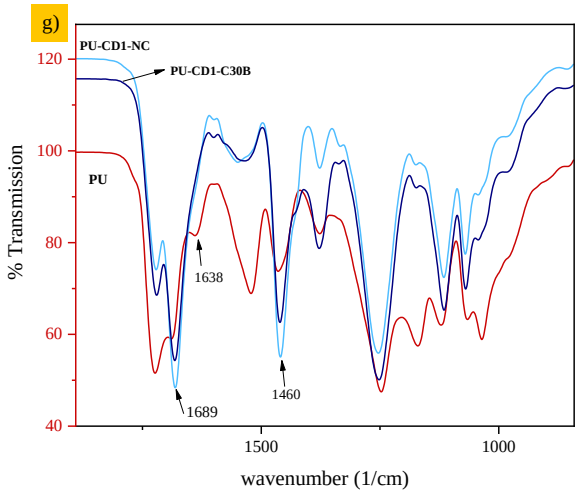
g)
PU-CD1-NC
PU-CD1-C30B
PU
1638
1460
1689
% Transmission
120
100
80
60
40
1500
1000
wavenumber (1/cm)

Fig.4 shows (a-c) Schematic illustration of PU incorporation with CD1 and its inclusion complexes forms hybrid nanofiller. a) PU-CD1, b) PU-CD1-NC and c) PU-CD1-C30B and (d-g) FTIR plot of PU and inclusion complex hybrid nanofiller based PU nanocomposite coatings.

Whereas the intensity of free C=O bond intensity is high as compared to bonded C=O for pristine PU. The absorption band at 2927cm^{-1} and 2857cm^{-1} corresponds to asymmetric and symmetric C-H stretching vibrations of CH2[40], is disappeared in CD1 and appeared in PU-CD1, PU-CD1-NC and PU-CD1-C30B confirming the C-H stretching vibrations due to the interactions with PU matrix. This implying hydrogen bonding affects the nano-interfaces. The peak at 1462 cm^{-1} corresponds to scissoring vibrations of C–H of CH_2, CH_3 deformation and CH_2 bending is prominent in PU-CD1-NC implies strong van der Waal bond formation in inclusion complex molecule[27,35]. The presence of these significant bonds in PU nanocomposites evident the hydrophobic physical interaction of CD1 and inclusion complex hybrid nanofillers with PU matrix (fig. 4(a-c)). Fig. 3 illustrated the schematic representation of the self-assembly arranged through the hydrophobic interactions. To get more insight of PU nanocomposites fabrication morphology analysis through FESEM and elemental analysis through EDS-mapping has been done.

Field emission scanning electron microscopy (FESEM) is a type of conventional scanning electron microscopy. It uses field emission gun as an electron generation system which enables it to provide micrographs at higher resolution system and superior energy range. In order to study morphology using FESEM samples made conductive for current. It has been done by sputtering the samples with a thin layer (1.5-3.0 nm) of platinum. The morphology, arrangement and elemental composition of all the specimens are analysed using FESEM.

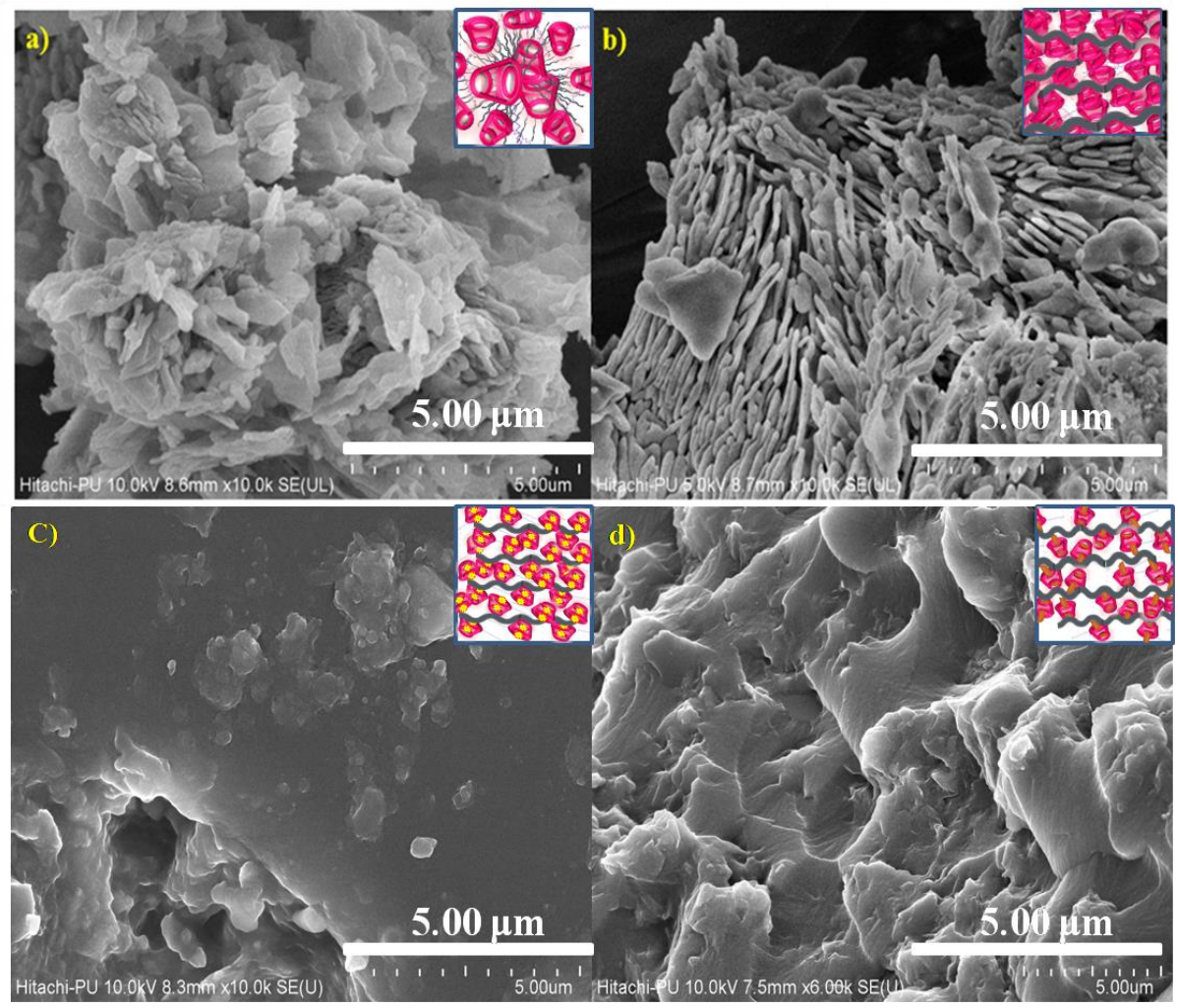

Fig.5. FESEM of a) CD1(inset shows the molecular structure of CD1), b) PU-CD1 (inset shows the self-assembly of PU-CD1), c) PU-CD1-NC (inset shows the self-assembly of PU – CD1-NC) and d) PU-CD1-C30B (inset shows the self-assembly of PU-CD1-C30B) nanocomposite coating samples.

Morphology of C30B and NC has been provided in supplementary data (fig.2 and 3), basis on which its presence is investigated in the FESEM of in-situ polymerized nanocomposite coatings. Fig. 5 displays the FESEM images of CD1 and PU-CD1 nanocomposites. FESEM images of PU-CD1 showed changes in the surface morphology of PU (polymeric matrices) with the dispersion of CD1.When the PU enters the CD1 cavity, its crystallinity is reduced due to the exfoliation and intercalation. This also changes the position and spatial structures of the CD1.Thus, their dispersion and physical interactions have been evidenced by FTIR and XRD. As shown in fig.5, the CD1 particles appear as flake-like crystals with a smooth surface (also confirmed from SEM images provided in supplementary data (fig.4)[41] (fig. 5a), and the inclusion of CD1 caused crystallites to grow in the immediate domain of the

surface. Through the technique of in situ polymerization, the CD1 has been enclosed in a polymeric matrix, as inferred from the FESEM images (fig. 5b). The shape of the particles in the PU-CD1 inclusion complex is obviously different from that of the β- cyclodextrin particles, and a flake-like structure with many lamellar crystals on the surface can be seen in fig. 5a. The change in the morphology of PU with inclusion of CD1 and the structural change in nanocomposite confirmed the formation of the PU-CD1 nanocomposite. Fig.5c shows the globular like structure[42,43] distributed on the surface of PU-CD1-NCsample. The incorporation of CD1 flake-like crystals with C30B clay sheets i.e., inclusion complex is dispersed in the PU matrix identify in fig.5d. Referring to schematic illustration of the self-assembly nanocomposites, (Fig. 4 (a-c). Further, the evaluation of elemental and mapping analysis confirmed the uniform distribution of the included elements in the synthesized coating films. Fig.6.displays EDS - mapping of CD1 and PU-CD1 nanocomposites. In the EDS mapping analysis image, all of the elemental species (carbon (C), oxygen (O), sodium (Na), sulfur (S)) utilized in the synthesis of CD1 and PU-CD1 nanocomposite are visible.

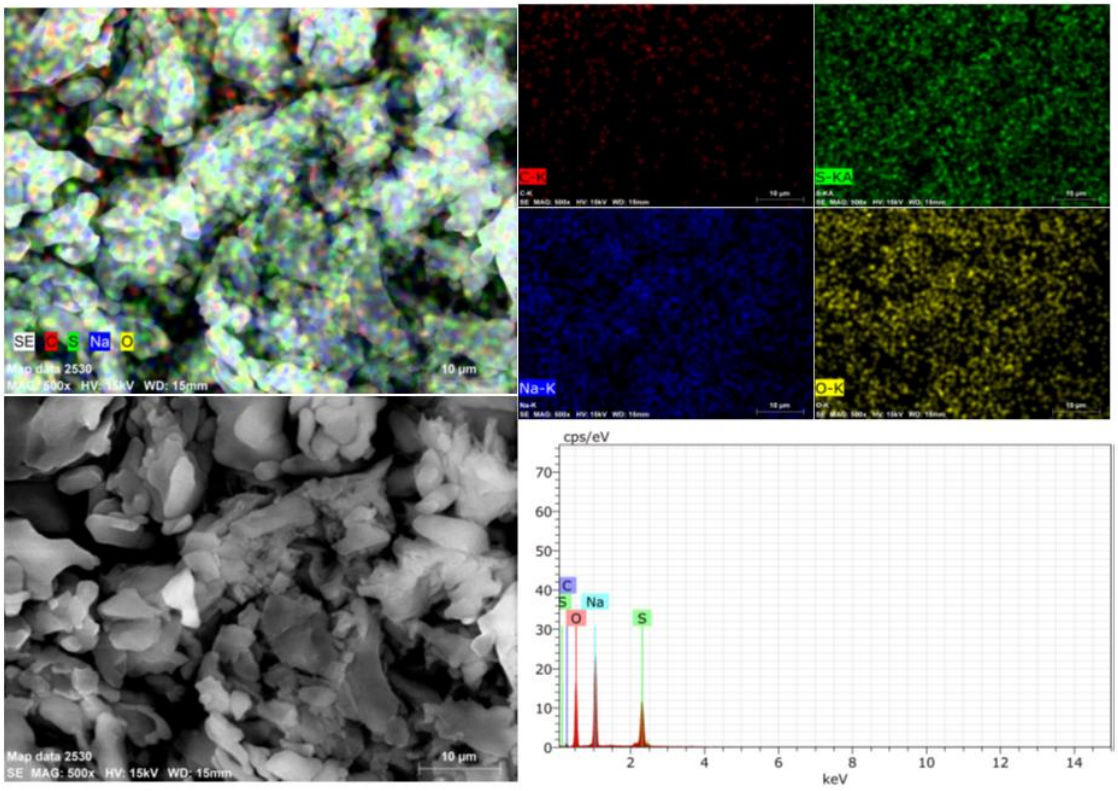

Fig.6. EDS and mapping of CD1 crystals

The mapping investigations revealed the uniform distribution of CD1 and its dispersion. The atomic percentage of C = 12.19, O=51.96, Na=25.91, S=9.94 for CD1 and C=30.09,

O=40.80, Na=18.41, S=10.71 for PU-CD1. This demonstrated the effective synthesis of CD1 and PU-CD1 nanocomposites with CD1 as the embodiment. The CD1 is composed carbon, sodium, oxygen and sulfur. Presence of sulfur and sodium in the elemental analysis confirms the interaction sodium undec-10-ene-1-sulfonate crystals attached to the heptakis-(6-deoxy-6-mercapto)-β-CD forming CD1.

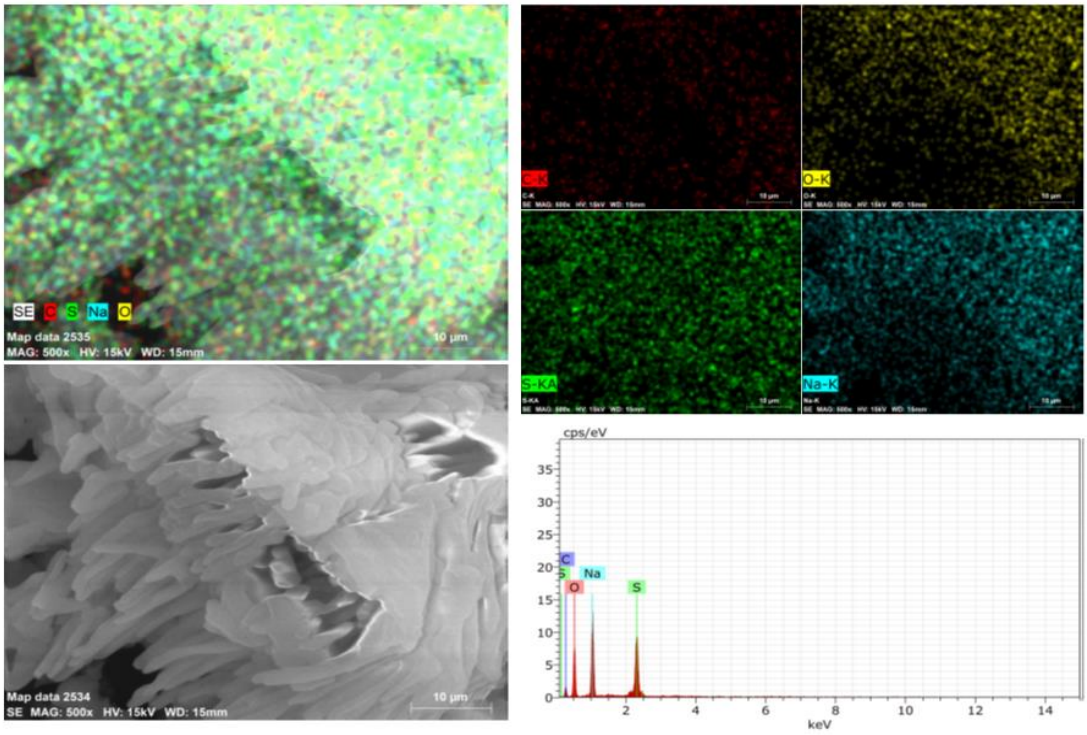

Fig.7. EDS and mapping of PU-CD1 nanocomposite coating

Upon reinforcement PU-CD1 a decrease in oxygen (40.80%) and sodium (18.41%), with an increase in carbon (30.09%) content, as PU is composed of carbon and hydrogen. It must be noted that FT-IR spectra of CD1 has affirmed this presence (fig.7).

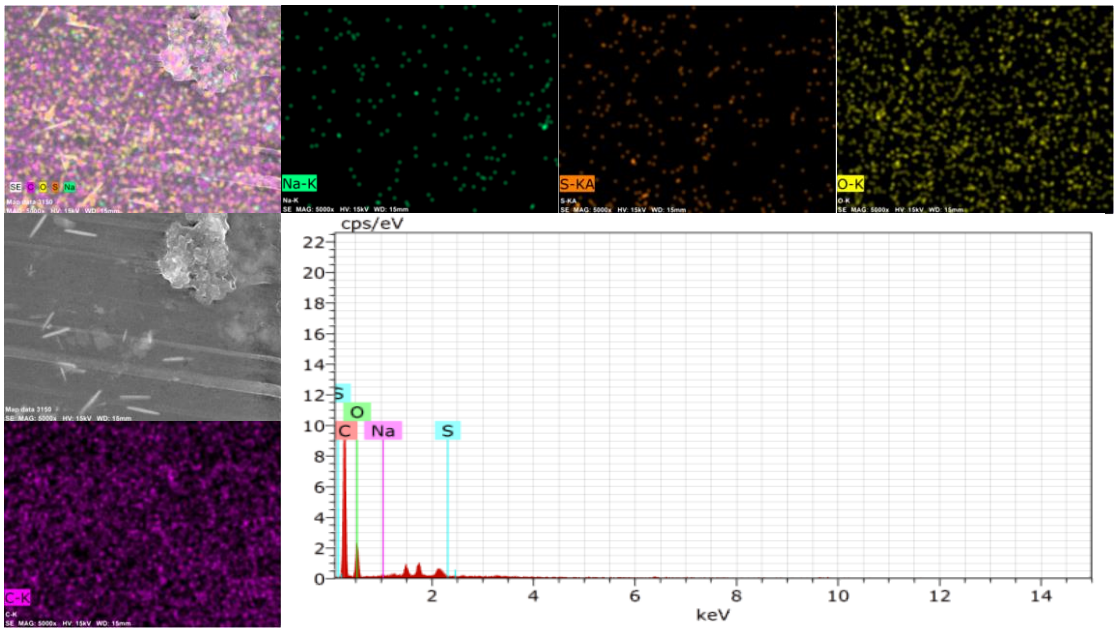

Fig.8. EDS and mapping of PU-CD1-NC nanocomposite coating

Incorporation of CD1 in an organic (i.e.,NC) component is done to fabricate a hybrid nanofiller which is more efficient for anti-microbial action. Then the hybrid nanofiller is integrated it in the PU matrix. The EDS spectra and elemental mapping of crystals PU-CD1-NC is displayed in fig.8. It shows the presence of C= 67.78%, O= 32.07%, S= 0.02% and Na= 0.12% atoms.

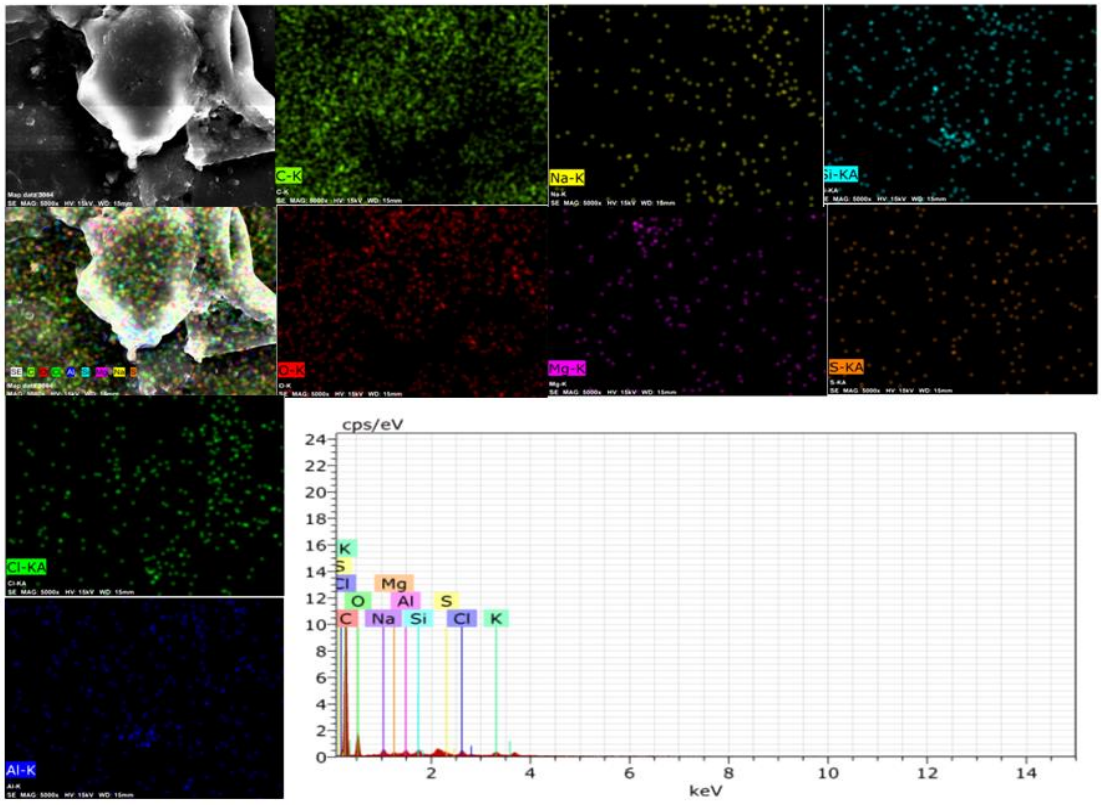

Fig.9. EDS and mapping of PU-CD1-C30B nanocomposite coating

Further to enhance the mechanical and thermal properties of a coating, C30B is integrated with CD1 for hybrid nanofiller and embedded in PU matrix. PU-CD1-C30B has the EDS spectra and elemental analysis shown in fig.9. The presence of Silica (0.36%), Aluminium (0.26%), sulfur (0.20%), chlorine (0.40%), magnesium (0.16%), potassium (0.43%), sodium (0.62%) and oxygen (19.66%). Due to the distinct crystalline structure of each of the analysed materials, the X-rays are dispersed by diffraction. From fig. 10a XRD pattern of sodiumundec-10-ene-1-sulfonate exhibits diffraction sharp peaks at 2θ = 19.9, 24.7, 29.3, 32.8, 34.8, 48.4, 59.7, 61.9 and 68.7 are in agreement with crystalline form.The sharpen of 19.9 peak[44] presence of sodiumundec-10-ene-1-sulfonate with few new sharp peaks confirms the synthesis of CD1 (fig.10b) by the addition of sodiumundec-10-ene-1-sulfonate to heptakis-(6-deoxy-6-mercapto)-β-CD[45].

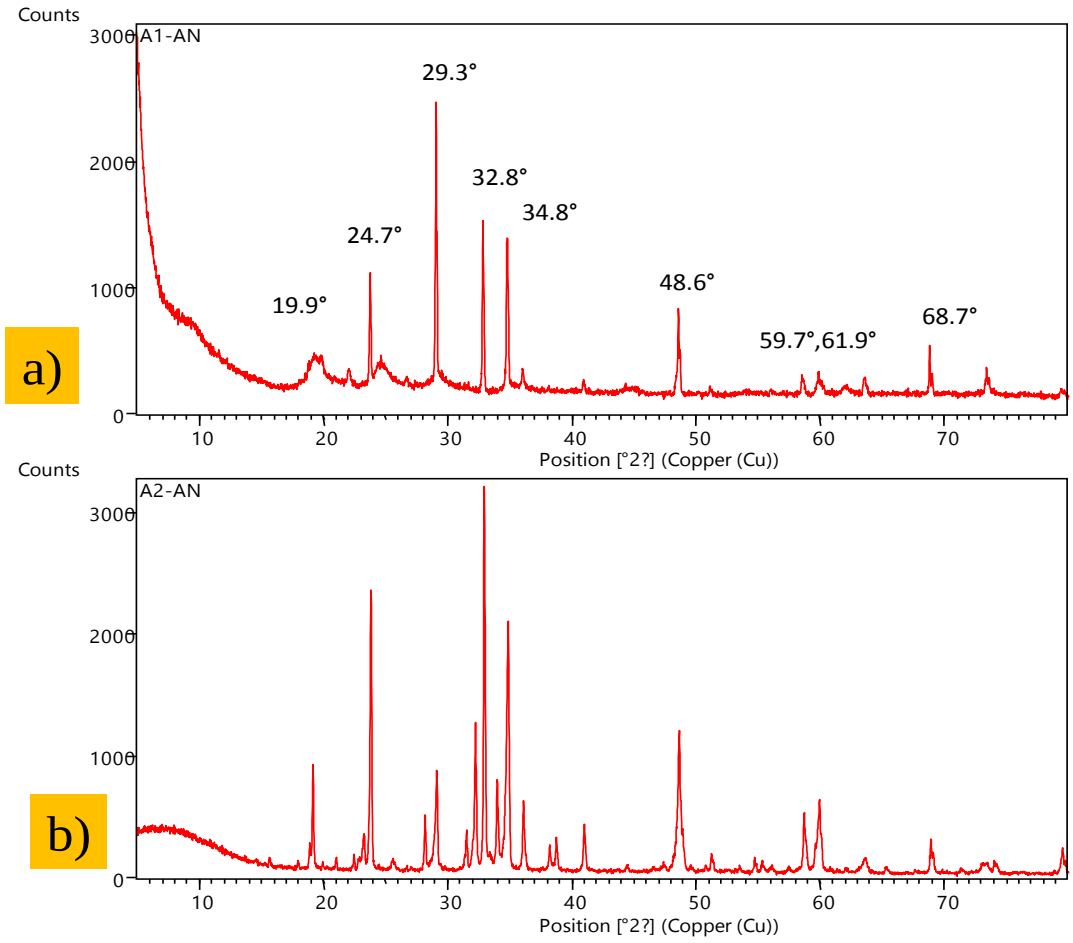

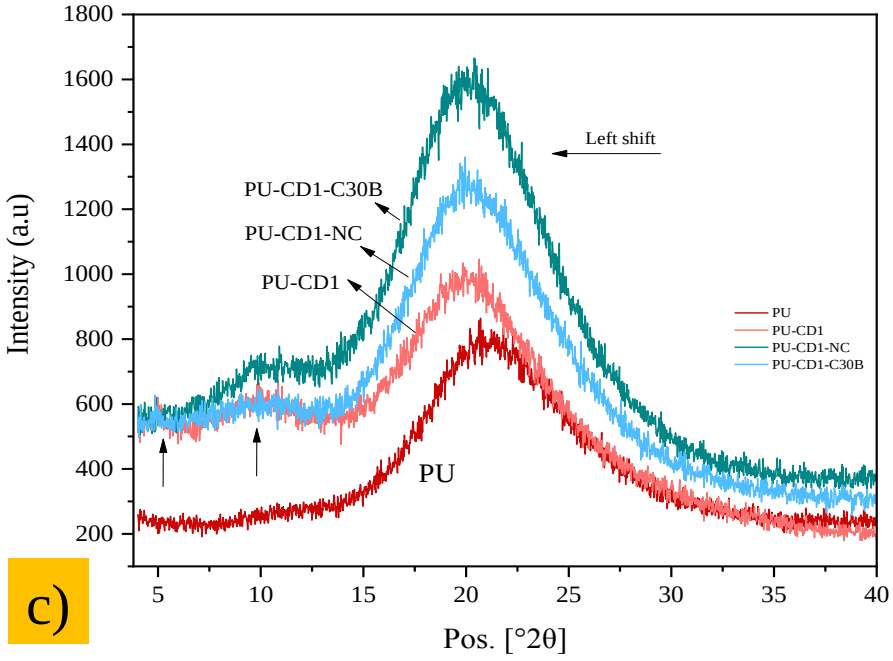

Fig.10. XRD OF a) sodiumundec-10-ene-1-sulfonate, b) CD1 and c) reinforced PU nanocomposite samples (PU, PU-CD1, PU-CD1-NC and PU-CD1-C30B).

In correlation to the morphological studies compared to the XRD pattern of the PU nanocomposites, the diffractogram (Fig.10c) indicates the presence of a new crystalline phase. Fig.10c represents the xrd plot of PU nanocomposites, the distortion of indicative peaks of heptakis-(6-deoxy-6-mercapto)-β-CD in PU-CD1 infers the exfoliation of the filler in the PU matrix[45,46]. Moreover, characteristic peaks at 2θ= 32°-37° present in sodiumundec-10-ene-1-sulfonate have resolved into 2 distinctive sharp peak in CD1 inferring the crystallographic arrangement, needle like crystallographic arrangement of sodiumundec-10-ene-1-sulfonate is evident from the product and microscopic images (supplementary data (fig.1)) and flake like crystals of CD1 from FESEM (fig.5a) and SEM images (supplementary data (fig.4)). Upon incorporation of CD1 with PU, reduced intensity of the characteristics peaks of filler, confirms the intercalation of CD1 in PU matrix, thus showing the amorphous nature. The peak absence in the scattering intensity curve exhibits the well dispersed and exfoliated morphology of PU matrix. However, the absence or low intensity of peak is a demonstrative proof of the exfoliation of the CD1 in the PU matrix, confirmed from FTIR and morphological studies. C30B has characteristic peak at 2θ of 4.78° , 9.664°, 19.63° and 21.95° with a d-spacing of 17.6 Å , 9.1425 Å, 4.5191Å and 4.046 Å. It has been seen in the

fig. 10 that PU shows a broader peak at 2θ of 19.63° which is due to the presence of some crystalline structure as PU chain's scattering with the regular inter-planar spacing[47–49]. In PU-CD1-C30B, there is a shift of broader peak and the characteristic peak of C30B has disappeared from the nanocomposite caused by the dispersion of inclusion complex in polymer matrix. In PU-CD1-NC, NC has the 2θ= 10° basal spacing of 8.83Å[50]. The characteristic diffraction peaks of the CD1 and NC disappeared in the xrd indicating disrupted oriented layers. The peak absence in the scattering intensity curve suggested well dispersed and exfoliated morphology of PU matrix (fig 4(a-c)).However, the absence of peak is not a demonstrative proof of the exfoliation or intercalation of the hybrid nanofiller but it can be inferred that it is due the disorientation of the hybrid nanofiller layers[51,52]. The embedment of the inclusion complex molecules as nanofiller in the PU matrix indicated the improvement in the chemical, thermal, water and mechanical resistance properties of the coatings.

Thermal properties

TGA is an analytical technique employed to determine the thermal stability of the material and its fraction of volatile components by tracking the weight change that occurs as the sample is heated at a constant rate. Fig 11depicts the TGA graph for the PU and nanofillers-based PU nanocomposites. The orange part highlighted depicted in Fig.11 shows the derivative graph of the bare PU and its nanocomposites which will help in providing a better understanding of the thermal properties for the same.

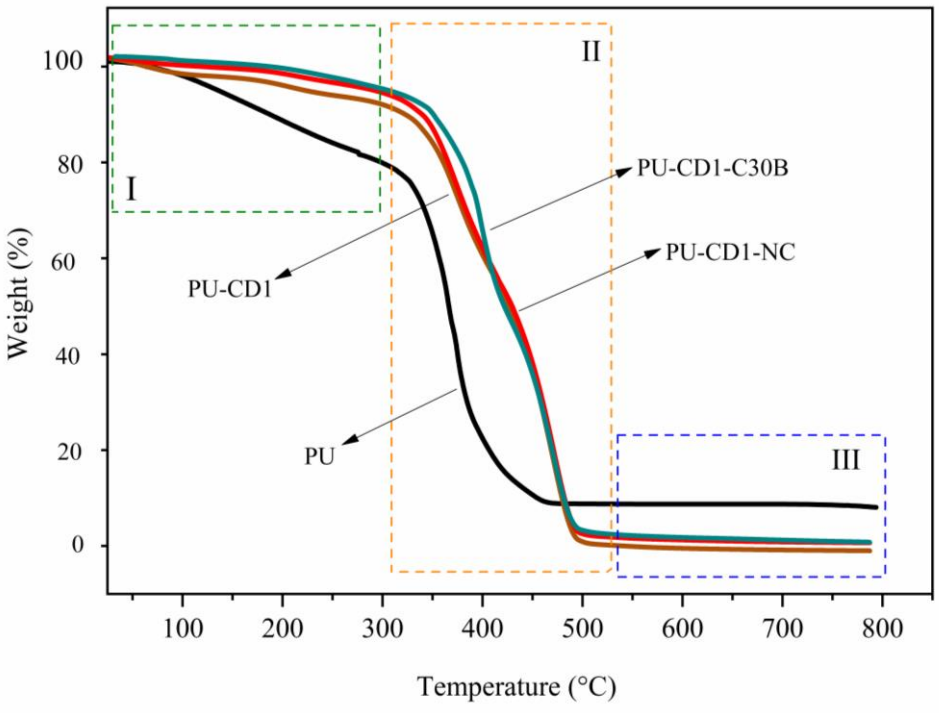

Fig.11. TGA plot of PU, PU-CD1, PU-CD1-NC and PU-CD1-C30B nanocomposite coating samples.

Table 2 compares the thermal characteristics of PU and PU nanocomposites based on nanofillers. Thermal investigations have shown that for pure PU and its nanocomposites, the sample degrades by 20% and 50%, respectively. The steepest TGA curve is used in the derivative curves to calculate the maximum level of deterioration relative to temperature. The first phase of Fig.11 shows the degradation of volatile substances like the solvent, and the second phase shows the maximum rate of mass loss for the degradation processes, which happens in the PU nanocomposites at temperatures of around 450°C (soft) and 350°C (hard). In comparison to bare PU, thermal deterioration in nanocomposite samples occurs at greater temperatures. This behaviour of nanocomposite samples can be explained by trapping of volatile compound between clay sheets (known as labyrinth effect) and attractive interface of PU-CD1-C30B[47]. These results are analogous to XRD, FTIR and FESEM studies.

Table 2:Thermal properties of PU and nanofillers based PU nanocomposites

S. No	Sample ID	20% Weight loss	50% Weight loss	Deviation from PU (20%)	Deviation from PU (50%)	Tp first derivative peak (soft phase)	Tp first derivative peak (Hard phase)	Deviation from PU (Soft)	Deviation from PU (Hard)
1	PU	338	365	0	0	364	375	0	0
2	PU-CD1	466	427	89	62	375	470	11	95
3	PU-CD1-NC	473	428	90	63	378	467	14	92
4	PU-CD1-C30B	468	420	82	55	397	471	33	96

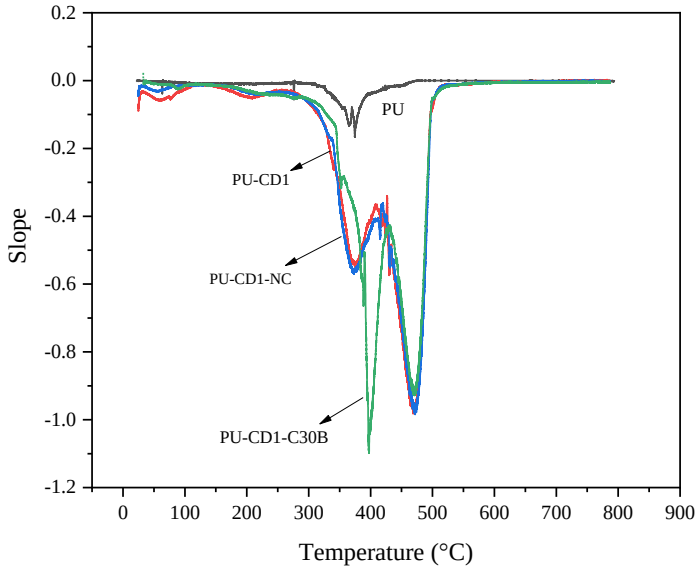

Fig.12. DTG curve of PU, PU-CD1, PU-CD1-NC and PU-CD1-C30B nanocomposite coating samples

The DTA and TGA curves of CD1 based PU nanocomposites are shown in Fig. 11 and 12. PU, PU-CD1, PU-CD1-NC and PU-CD1-C30B presented three stages of weight loss (Fig.12). The first stage is recorded at 80-120°C. The weight loss at this stage indicates the loss of volatile components. PU nanocomposites showed enhanced thermal stability (~200 °C temperature difference) than pristine PU. Nanocomposites exhibited their first peak at 380 °C, due to dihydroxylation of OH groups of NC molecules decomposition of PU-CD1-NC[53]. Fig 12 exhibits the decrease in weight loss of PU-CD1-NC due to strong physical interaction at the interface of NC. Also, the developed NC integrated with CD1 has improved thermal stability due to its crystalline nature. Consequently, for PU-CD1 and PU-CD1-C30B samples the weight loss found at 380 °C infers the decomposition of CD1 structure because of its transition from solid to liquid phase. Also the addition of C30B to CD1 has enhanced the thermal barrier property. Relatively slow weight decomposition at 470 °C is due to the thermal degradation of “char”, a residue formed during the second stage of nanocomposite decomposition[54]. Amorphous solids soften gradually once heated and tend to have a relatively wide range for melting point, a zone between solid and liquid phase.C30B loaded sample performed inferior among all the samples benefited from the inherent properties of C30B. It is clear from the thermal degradation analysis that along with dispersion status, phase morphology and polymer-filler interface at the micro and nano scale significantly affect the performance properties of bulk and surface[55]. The degradation is divided in the

following parts volatiles, de-polymerization (hard & soft), secondary reaction. De-polymerization phase temperature is calculated from DTG curves of PU and PU nanocomposite. The data is tabulated in Table 2 and the degradation phases are shown in fig.12.In comparison to PU thermal degradation of hard segment has been increased by approx 95°C and 20% weightloss by approx 85°C. Initial thermal resistance is provided by the PU matrix and guest molecules linked with the PU and inclusion with the CD1. In fact the presence of C30B raised the soft segment degradation by 33°C. NC being an organic compound consists of carbon hydrogen composition disrupt early than C30B inclusion complex[41]. Increase in the resistance of both hard and soft segments take place, as the physical chemical cross linking makes urethane linkages stronger and more resistance to thermal decomposition, while the barrier properties delay the escaping vapours of soft segments[56]. These attributes are yet again dependent on dispersion of nanofillers. Further restricted mobility of the PU chains due to C30B platelets especially the soft segment also accounts for the delayed thermal decomposition. The hard segments as corroborated from XRD and FTIR studies forms cluster of ordered hard domains.

Fig.13 displays the flame retardance histogram of PU, PU-CD1, PU-CD1-NC and PU-CD1-C30B.The flame retardant mechanism of PU nanocomposite is connected with two critical factors: One is the thermal-oxidative deterioration of the matrix, and the other is the condensed-phase diffusion of volatile breakdown products.The carbonaceous char that forms on the surface while burning acts as a barrier against heat and mass transmission, which is how flame retardants work[56,57]. The presence of C30B have enhanced the flame retardance time due to the presence of inorganic C30B layer hinders the intumescing behaviour in coating. It is due to the barrier effect of exfoliated layered silicates for volatiles in the nanocomposites, crucial in delaying thermal-oxidative degradation[56]. PU-CD1 and PU has the approx. similar value of flame retardance infers the well dispersed and intercalated composite coating. PU-CD1-NC has the lowest flame retardance value, due to the presence of excess amount of oxygen in NC, also confirmed from EDS results.

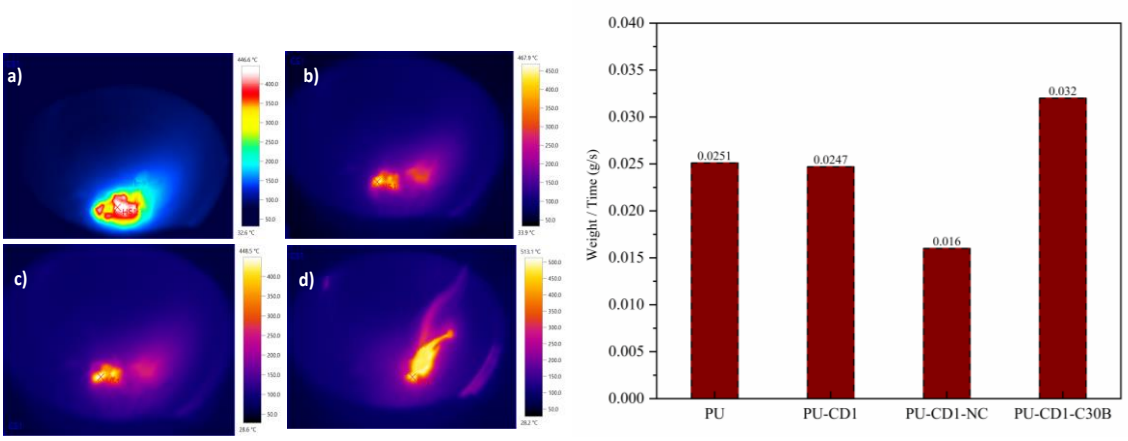

Fig.13. Flame retardance IR images after a) PU, b) PU-CD1, c) PU-CD1-NC and d) PU-CD1-C30B nanocomposite coating samples (on left) and weight loss withtime histogram of PU, PU-CD1, PU-CD1-NC and PU-CD1-C30B nanocomposite coating samples (on right).

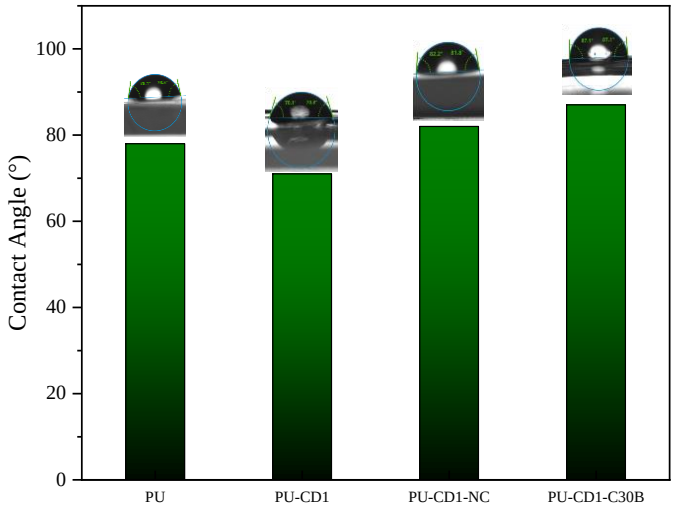

Fig.14. Contact angle of PU, PU-CD1, PU-CD1-NC and PU-CD1-C30B nanocomposite coatings.

To explore wettability of the PU nanocomposites, water contact angle (WCA) of coatings PU, PU-CD1, PU-CD1-NC and PU-CD1-C30B has been examined. Fig.14 PU, PU-CD1, PU-CD1-NC and PU-CD1-C30B displayed water contact angle of 78°, 70°, 81.8°, and 87.1° respectively. Amongst all the coating samples, PU-CD1-C30B sample exhibited highest WCA (87.1°) which showcasesits hydrophobic nature. This hydrophobicity demonstrated by PU-CD1-C30B sample is credited to lack of polarity due to presence of dispersed filler in the PU matrix infers the carbon atoms in its structure and adsorption of hydrocarbons from air which causes decrease in the surface energy of the substrate thereby increasing its hydrophobicity[58]. Improvement in WCA of the nanocomposite samples in comparison to

pristine PU infers the well dispersion of hybrid nanofiller in the PU matrix. High contact angle value also shows smoothness in coating topology. PU-CD1-NC sample exhibited WCA of 81.8° which states its intrinsically hydrophilic nature as compared to other samples. The hydrophilicity can be attributed to the presence of abundant hydrophilic oxygen moieties incorporated in the morphology of PU-CD1-NC[59]. FT-IR results of PU-CD1-NC mentioned in fig.4 also confirmed presence of low dispersion of H-bonded groups that are in turn responsible for the increased hydrophilicity of the synthesised PU-CD1-NC. Then PU-CD1 has the lowest contact angle can explains the hydrophilic interactions capability due to its amphiphilic structure. Similar results have been reported in literature where presence of partially negative functional groups has contributed to higher hydrophilicity. To get the insight of coatings behaviour towards chemical stability, relative THF absorption and relative water absorption for comparison have been investigated.

The results from contact angle results showed the amount of hydrophobic content (fig.15) whereas the immersion results tell us the amount of absorption, retention and release of water and THF content from our samples. Here, values are taken after 1 hour for four consecutive times, as no such change is observed in consecutive 1hour readings thereafter certain random readings are taken to observe the changes.

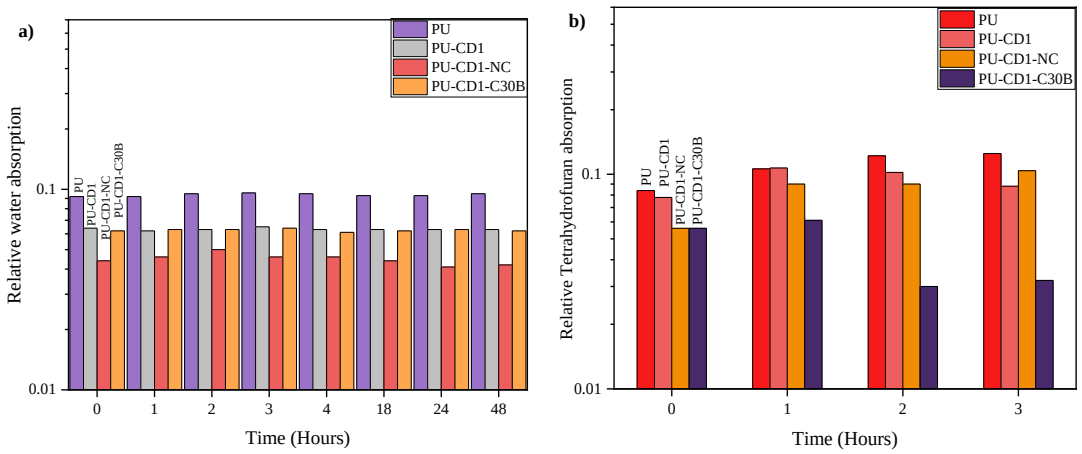

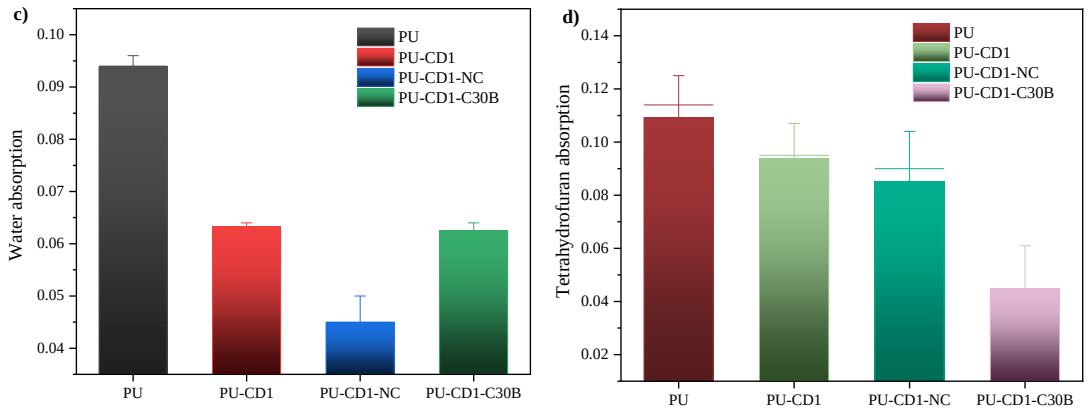

Fig.15a) Relative water absorption of hybrid nanofiller based PU nanocomposite coatings, b) Relative tetrahydrafuran absorption of hybrid nanofiller based PU nanocomposite coatings, c) water absorption and d) tetrahydrafuran absorption for 48 hours of hybrid nanofiller based PU nanocomposite coatings.

From fig. 15 it is noted that the presence of NC to PU-CD1 has slower absorption of water relative to pristine PU due to the presence of H+ caused due to the release of OH^{-} in the immersion by inclusion complex formed by the nanofiller in the CD1 cavity[60]. In relative absorption study PU-CD1-NC showed greater water absorption resistance capacity and PU-CD1-C30B exhibited highest relative THF absorption resistance capacity is observed. In fact the presence of CD1 has high resistance towards water absorption in comparison to THF absorption. Nanofillers-based PU nanocomposites performed better than bare PU. The amount of absorption of each sample is as follows: for CD1 based hybrid nanofiller based nanocomposites –for water PU-CD1-NC<PU-CD1-C30B=PU-CD1<PU and for THF PU-NC-C30B<PU-CD1-NC<PU-CD1<PU(fig.15 c-d).The presence of C30B to PU-CD1 has slower absorption of THF relative to pristine PU. The hybrid nanofiller based PU nanocomposite coating films release the H+, hydrogen bond gets easily targeted during the disruption of PU hybrid nanofiller composite coatings[61]. The decrease in the absorption capacity reveals the distortion of bonds and causes the breakdown of nanocomposite coatings. PU-CD1-C30B has the lowest relative absorption due to the better dispersion of the hybrid nanofiller and strong interfacial interactions between C30B and CD1. PU has the highest absorption of THF which exhibits its easy breakdown in the basic nature due to weak interfacial interactions. In accordance to this behvaior, weakening of hydrogen bonds has been investigated using tensile testing.

Mechanical properties

The ultimate tensile strength (UTM) of all the hybrid nanofiller based PU nanocomposite films are enhanced compared to the pristine PU. According to previous work, incorporation of C30B led to increase in the UTM of PU-C30B nanocomposite films, while the toughness of all the films is higher than the pristine PU. It can be clearly related to the presence of CD1, hybrid nanofillers and its interactions with PU chains. It is interesting to mention that the yield strength of PU nanocomposite containing C30B and CD1 is higher than pristine PU. It is related to the high interaction and rigidity of chains in the PU matrix. The UTS of PU, PU-CD1, PU-CD1-NC and PU-CD1-C30B are1.28, 23.32, 17.09, 18.61MPa respectively(table3). Strong hydrogen bonds, C-O-NH, and other dipole-dipole interactions provide high tensile strength coupled to a long linear PU chain, resulting in high tensile elongation [38].

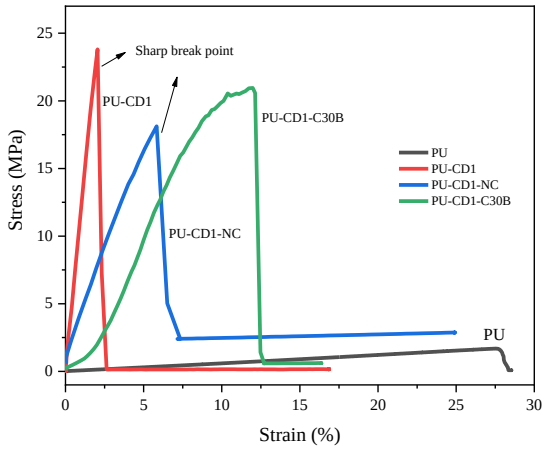

Fig.16. Stress-strain curves for PU, PU-CD1, PU-CD1-NC and PU-CD1-C30B nanocomposite coatings.

Table 3: Mechanical properties of the coatings

S.No	SAMPLE ID	UTS (MPa)	0.2% Strain, yield stress (MPa)	Toughness (N-mm)	Elongation at break (%)
1	PU	01.28	00.42	23.79	33.01
2	PU-CD1	23.32	11.10	30.42	18.37
3	PU-CD1-NC	17.09	15.51	71.09	28.26
4	PU-CD1-	18.61	18.71	111.47	17.79

Model fitting:

The model fitting, is a theoretical way to predict the interfacial characteristics at the nano level. Theoretical assessment of mechanical and thermal characteristics of CD1 and hybrid nanofiller-PU nanocomposites samples have been done using Callister model. Theoretical analogy between thermal and mechanical performance is evaluated by modifying the Callister model for thermal plots.

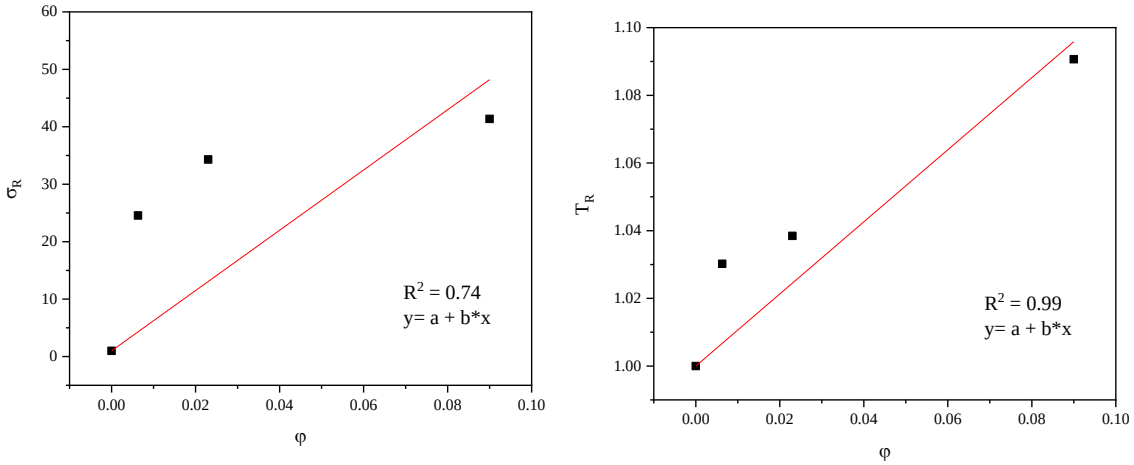

Fig.17 plot of relative yield strength vs volume fraction (eq.1 on left) and relative derivative temperature vs volume fraction (eq2 on right) for an average value of α =500nm.

Callister model has been used to depict the interfacial strength of polymer nanocomposites by calculating "S" value (eq.1 & 2), value of "S" stands for interfacial stress parameter infers the strength of interactions at nano level. Callister model has been applied to yield stress valuesand modified for thermal results to correlate the experimental and theoretical observations of both thermal and mechanical performance of the coatings. Experimental results are in good agreement with theoretical plot. Relative soft segment derivative curve temperature is plotted against the filler volume for calculate the "S" strength parameter for average value of α =500nm. For thermal analysis S= 1.5 and similarly for mechanical analysis S=0.5.The positive value of S, infers the better performance of coatings due to strong interfacial interactions[62],to obtain its theoretically positive value, it must lie under one of these conditions a) negative slope must be less than 1 or b) positive slope will always exhibit the positive value of S. In fig.18 a, b the relative values are increasing with the increase in

volume fraction infers improved interfacial strength. It also signifies the analogy of the thermal and mechanical mathematical analysis.

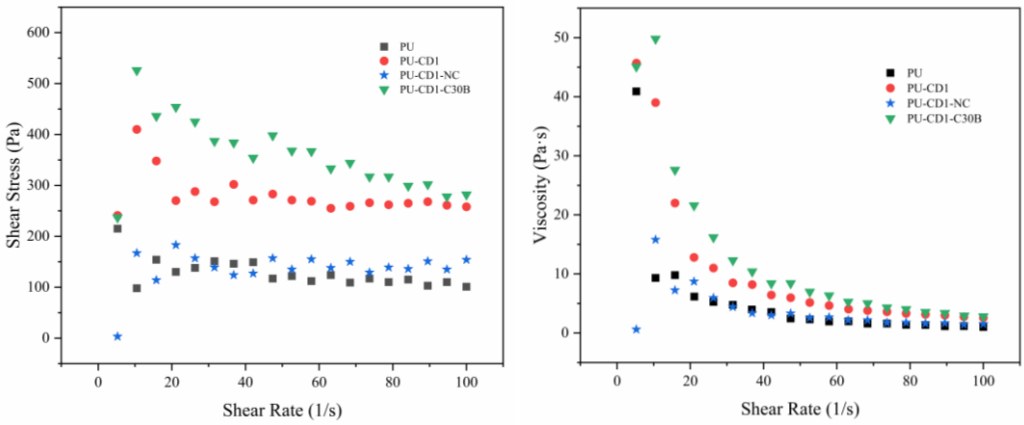

Fig.18. Plot of shear rate and shear stress for PU and PU nanocomposite (on left) and plot of viscosity vs. rate for PU and PU nanocomposites (on right)

PU nanocomposite samples have shear thinning characteristics, the viscosity of nanocomposite suspension has decreased with the increase in shear rate. There is a maximum viscosity of 50 Pa.s in PU-CD1-C30B which decreases as the shear rate increases, resulting in a shear thinning behaviour in PU-CD1-C30B. Integration of C30B in the nanocomposite tends to exhibit maximum viscosity at first among all the samples (fig. 18). The incorporation of CD1 and hybrid nanofillers to the anti-microbial suspension leads to a shear thinning behvaior. Viscosity is very high at low shear rates and decreases progressively at higher shear rate for PUnanocomposites[63]. It depends upon various parameters such as dispersion of filler in the matrix, orientation, filler content, particle - particle and filler matrix interactions. This initial rise in viscosity is indicative of the higher intensity of interfacial interactions offiller and its dispersion in the matrix. During the flow the C30B sheets aligned itself to the flow, the disruption in the orientation or restriction in the aligned orientation, the viscosity tends to decrease, thus showing compliance in flow[64]. Also the attachment of NC attached to the CD1 hinders the orientation of hybrid filler towards the direction of flow.

According to Fig.19, PU-CD1-NC, PU-CD1, PU-CD1-C30B along controlled sample (C) i.e., PU and AB as anti-biotic (Amoxicillin) showed antibacterial activity against gram-positive (S aureus) and gram-negative (*E. coli*) bacteria. Hybrid nanofiller-PU samples have better antibacterial activity against *E.coli* than S. aureus. Anti-bacterial activity against gram-negative *E.coli* showed zone of inhibition (ZOI) of 1.8cm, 3cm, 2.2 cm, for S2, S3, and S4 samples and gram-positive *S.aureus* bacteria showed zone of inhibition (ZOI) 1.7cm, 2.7cm,

2.6cm for S2, S3, and S4 samples (supplementary fig.5). The results also indicated that sulfonated group attached to heptakis-(6-deoxy-6-mercapto)-β-CD have increased the antibacterial activity. Cyclodextrins have numerous hydroxyl groups at each end and create a toroid (truncated cone) shape. This enables them to encapsulate hydrophobic molecules[27].

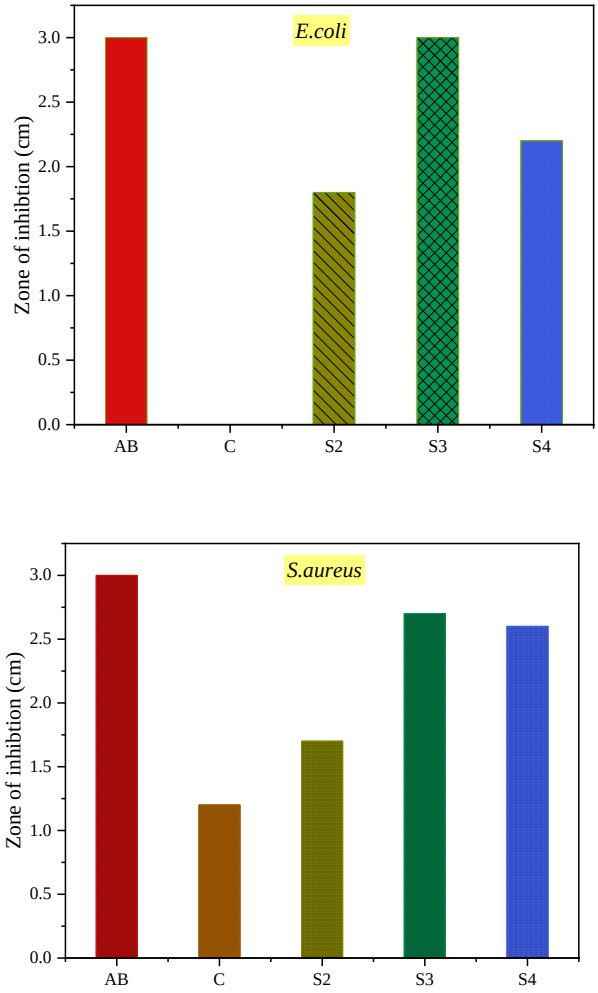

Fig.19. Displays the histogram of zone of inhibition of well diffusion assay by incubating coating samples S2: PU-CD1-NC, S3: PU-CD1 and S4: PU-CD1-C30B1 against gram negative bacteria *E.Coli* and gram-positive bacteria *S.aureus*. C: Controlled Sample (PU) and AB: Anti biotic (Amoxicillin)

The results of *in-vitro* bacterial resistance test showed that CD1 complexed with other fillers and incorporated with hydroxyl group of PU exhibited significant inhibition of *E. coli* and *S.aureus* growth even at the lowest weight percentage i.e., 1wt.%, which is attributed to a well dispersed formulation of hybrid nanofiller in uncured suspension. PU, a controlled sample has also displayed resistance against gram-positive bacteria, which gets enhanced

upon addition of hybrid nanofiller. The antibacterial impact of uncured PU-CD1-NC and PU-CD1 against *E. coli* and *S. aureus* appears to be related to the contact of the bacterial cell's outer membrane, lipopolysaccharide, or other biomolecules[50].It is most likely the vulnerable location to cyclodextrins and their derivatives. Recent findings revealed that the additional antibacterial properties of β-CDs, show significant potential to limit bacterial activities by modifying their quorum sensing.

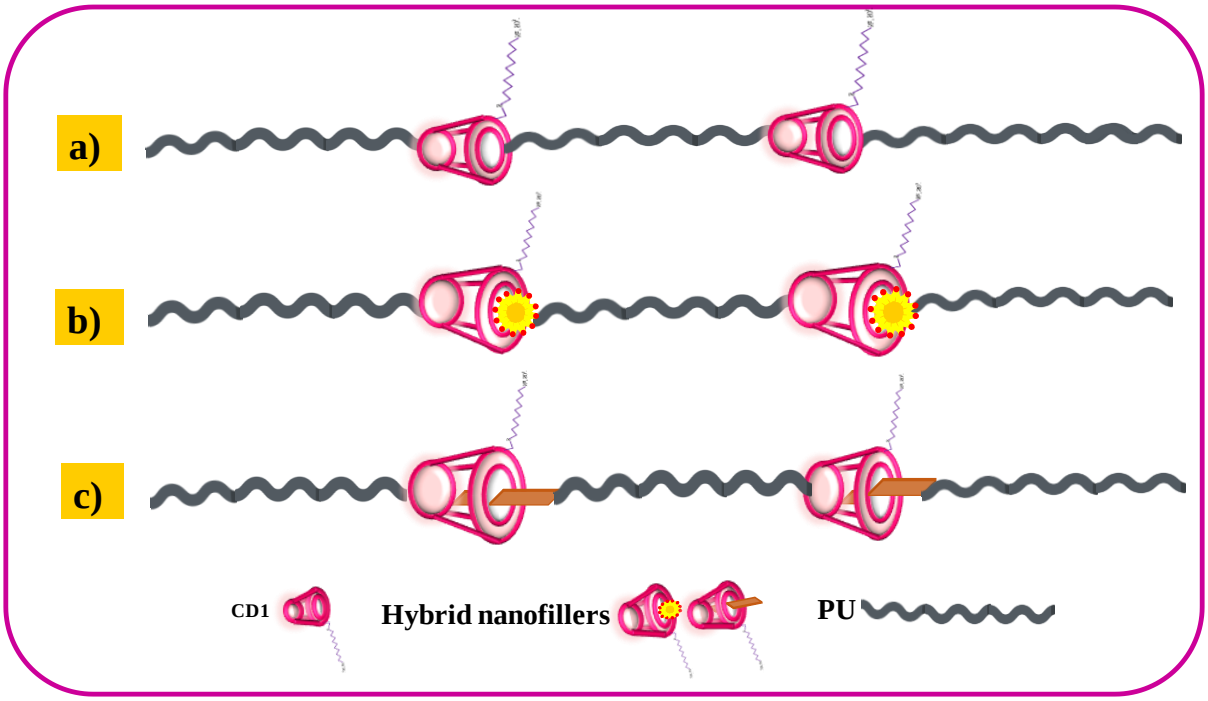

Fig. 20 displays the illustration of PU incorporation with CD1 and hybrid nanofiller

The guest molecule bonds the hydrophobic interactions with the host molecule forming the inclusion molecules. The incorporation of CD1 in PU matrix improved the anti-bacterial resistance against gram negative bacteria and improved its degradation against water and THF absorption. Addition of CD1 to PU has drastically changed the nature of the coating from plastic material to glassy material with the addition of CD1 to PU; this has changed to a tough and elastic behaviour by using inclusion complex molecules as hybrid nanofiller (fig.20). A sharp peak in the thermal degradation of PU-CD1-C30B indicates the enhancement in the thermal degradation resistance temperature of the PU coating. Zone of inhibition in the well diffusion test confirm the bacterial resistance of the suspension. Host-guest incorporation of the CD1 with NC and C30B synthesized hybrid nanofiller that exhibitschemical, philic, thermal and mechanical resistance properties when embedded in the PU matrix. The PU-hybrid nanofiller interactions and its impact on the coating performance have been summarized here.

1)FTIR spectra revealshydrophobic interactions between the host and guest as well as non-covalent bonding forces such as hydrogen bonding and van der Waal forces are the main driving forces in the synthesis of inclusion complex of CD1 with NC and C30B (fig.1 & 3). Its embedment into PU matrix through hydrogen bonding interactions (fig.4) affects the nano-interfaces exhibiting reduced intensity of filler characteristics peaks, confirming the intercalation of CD1and hybrid nanofiller in PU matrix, thus showing the amorphous nature in XRD (fig.10).

2) During in-situ polymerization, the diol component of the PU has the affinity to form vander Waal forces especially hydrogen bonding with the CD1 and its inclusion complexes, its uniform dispersion over the PU matrix as observed in FESEM (fig.5),indicated by EDS mapping (fig 7-10) and illustrated schematically in fig.20.

3)Through thermal (fig.11 & 12) and flame retardance analysis it has been observed that the decrease in weight loss of PU-NC-C30B and PU-CD1-NC is due to strong physical interaction at the interface of hybrid nanofiller. The dispersion level, phase morphology and polymer-filler interface at the micro and nano scale (fig.4 & 15) significantly affect the coating performance at both bulk and surface level.

4) Incorporation of CD1 as a nanofiller in the PU matrix has been done to develop contact-killing anti-bacterial surface (fig.19) supported by the rich chemistry of the PU due to its urethane linkages and affinity to strong interactions. However, the sharp break peak (fig.16) seen in the tensile results indicates its glassy nature which makes it difficult to support underlying material during the exposure to the application.

5) To develop a thermally and mechanically stable coating, C30B and NC has been added to anti-bacterial CD1 through host-guest interactions and its integration in the PU matrix exhibited a multifunctional coating with 78% rise in toughness with the addition of C30B and ultimate tensile strength by 15%.In terms of water and THF absorption resistant performanceof coating (fig.15) showed the PU-CD1-NC and PU-CD1-C30B exhibited lowest absorption of water and THF respectively, even recorded after 48 hours.

6) Callister model fitting to the experimental results showed an analogy among experimental and theoretical analysis. Increase in yield stress value with the increase in volume fraction exhibited positive interfacial stress transfer parameter value (fig.18a). It infers the improved stiffness of the PU nanocomposite coatings with the addition of NC and C30B.

7) Modified Callister model has been applied to TGA results and it is in goodagreement with the experimental values with R^2 = 0.99 (fig.18b). It also demonstrates an analogous trend to mechanical results. The outcomes evident the experimental performance of coatings, for instance the "S" value is positive for TGA results, infers the improvement in thermal degradation resistance with the increase in volume fraction. Upon evaluation of model fitting and experimental performance of samples, it is revealed that the addition of C30B has exceptionally improved the mechanical and thermal performance of coating.

These points make this coating very much suitable for the bio-implants and bio material surface coatings. The inclusion of nanoparticles in the cavity of CD1 enhanced the materials' properties and its nanocomposite exhibits the strong chemical, thermal and mechanical resistance to support the underlying material and over the surface supports the bacterial resistance thus turning these into multi-functional coatings.

Conclusion:

In this work, a feasible and simple approach has been applied to synthesise a multifunctional coating by embedding the inclusion complexes (hybrid nanofiller) in the PU matrix. Supramolecular interactions within the inclusion complex resulted in formation of multifunctional coatings. These coatings exhibited water resistant, thermally and mechanically stable performance. Additionally, it revealed an irreversible mechanism of action against gram-positive and gram-negative bacteria. Upon evaluation of the performance of these multifunctional coatings, it is suggested that these coating are effective for the application at frequently exposed surfaces that are sensitive to bacterial growth, abrasion, thermal expansion and weathering, like those in public hospitals.

Declaration of Competing Interest

The authors declare that they have no known competing financial interests or personal relationships that could have appeared to influence the work reported in this paper.

Acknowledgement

The authors thank Covestro (India) Private Limited for providing us with the necessary materials on- gratis. We acknowledge the contribution of SAP (UGC, New Delhi), PURSE

(DST, New Delhi) and TEQIP-III grants accorded to Dr. SSBUICET. We acknowledge the financial assistance given by DST-UT (S&T&RE/RP/147/Sanc/09/2017/1123-1129 and S&T&RE/RP/147/e-2873/(22-23)/Sanc/09/2022/907-915) and DRDO (DMSRDE Kanpur) (TR/0569/CARS-130 dated 16/12/2021). We acknowledge the receiving of collaborative grant from Nottingham Trent University (NTU), United Kingdom under the science and technology initiative.

References:

[1] A. Atiqah, M. M.T., B.A. Ali, M. Jawaid, S. Sapuan, A Review on Polyurethane and its Polymer Composites, Curr. Org. Synth. 13 (2016) 1. https://doi.org/10.2174/1570179413666160831124749.

[2] M. Nayani, S. Gunashekar, N. Abu-zahra, Synthesis and Characterization of Polyurethane-Nanoclay Composites, 2013 (2013).

[3] A. Sharma, M. Babar, P. Kakkar, P. Gahlout, G. Verma, Correlating mechanical properties of polyurethane-organoclay nanocomposite coatings with processing, Prog. Org. Coatings. 169 (2022) 106895. https://doi.org/10.1016/j.porgcoat.2022.106895.

[4] D. Monomers, I. V Khudyakov, Polyurethane Nanocomposites, (2018). https://doi.org/10.1163/156855509X448253.

[5] G. Verma, A. Kaushik, A.K. Ghosh, Preparation, characterization and properties of organoclay reinforced polyurethane nanocomposite coatings, J. Plast. Film Sheeting. 29 (2013) 56–77. https://doi.org/10.1177/8756087912448183.

[6] G. Verma, A. Kaushik, A.K. Ghosh, Progress in Organic Coatings Nano-interfaces between clay platelets and polyurethane hard segments in spray coated automotive nanocomposites ., Prog. Org. Coatings. 99 (2016) 282–294. https://doi.org/10.1016/j.porgcoat.2016.06.001.

[7] Y. Chen, J. Yan, Y. Zhang, W. Chen, Z. Wang, L. Wang, Synthesis , Characterization and Antibacterial Activity of Novel β‐cyclodextrin Polyurethane Materials, J. Polym. Environ. 30 (2022) 1012–1027. https://doi.org/10.1007/s10924-021-02255-7.

[8] S. Brzeziński, G. Malinowska, T. Nowak, H. Schmidt, D. Marcinkowska, Structure and Properties of Microporous Polyurethane Membranes Designed for Textile-

Polymeric Composite Systems, 13 (2005) 53–58.

[9] Materials Science and Technology Polyurethane / M-MMT coating : investigation of anticorrosion , antimicrobial , mechanical and thermal properties, (n.d.).

[10] D. Park, A.M. Larson, A.M. Klibanov, Y. Wang, Antiviral and antibacterial polyurethanes of various modalities, Appl. Biochem. Biotechnol. 169 (2013) 1134–1146. https://doi.org/10.1007/s12010-012-9999-7.

[11] S.M. Imani, L. Ladouceur, T. Marshall, R. Maclachlan, L. Soleymani, T.F. Didar, Antimicrobial nanomaterials and coatings: Current mechanisms and future perspectives to control the spread of viruses including SARS-CoV-2, ACS Nano. 14 (2020) 12341–12369. https://doi.org/10.1021/acsnano.0c05937.

[12] B. Balasubramaniam, Prateek, S. Ranjan, M. Saraf, P. Kar, S.P. Singh, V.K. Thakur, A. Singh, R.K. Gupta, Antibacterial and Antiviral Functional Materials: Chemistry and Biological Activity toward Tackling COVID-19-like Pandemics, ACS Pharmacol. Transl. Sci. 4 (2021) 8–54. https://doi.org/10.1021/acsptsci.0c00174.

[13] Z. Zhang, V.E. Wagner, Antimicrobial coatings and modifications on medical devices, Antimicrob. Coatings Modif. Med. Devices. (2017) 1–273. https://doi.org/10.1007/978-3-319-57494-3.

[14] X. Li, T. Huang, D.E. Heath, N.M. O'Brien-Simpson, A.J. O'Connor, Antimicrobial nanoparticle coatings for medical implants: Design challenges and prospects, Biointerphases. 15 (2020) 060801. https://doi.org/10.1116/6.0000625.

[15] C. Wang, C. Mu, W. Lin, H. Xiao, Functional-modi fi ed polyurethanes for rendering surfaces antimicrobial : An overview, Adv. Colloid Interface Sci. 283 (2020) 102235. https://doi.org/10.1016/j.cis.2020.102235.

[16] Z. Zhang, V.E. Wagner, Antimicrobial coatings and modifications on medical devices, 2017. https://doi.org/10.1007/978-3-319-57494-3.

[17] M. Cloutier, D. Mantovani, F. Rosei, Antibacterial Coatings : Challenges , Perspectives , and Opportunities, Trends Biotechnol. 33 (2015) 637–652. https://doi.org/10.1016/j.tibtech.2015.09.002.

[18] G. Verma, Polymer nanocomposites and coatings: The game changers, Trends Appl. Adv. Polym. Mater. (2017) 1–22. https://doi.org/10.1002/9781119364795.ch1.

[19] G.J.A. Ter Boo, T. Schmid, I. Zderic, D. Nehrbass, K. Camenisch, R.G. Richards, D.W. Grijpma, T.F. Moriarty, D. Eglin, Local application of a gentamicin-loaded thermo-responsive hydrogel allows for fracture healing upon clearance of a high Staphylococcus aureus load in a rabbit model, Eur. Cells Mater. 35 (2018) 151–164. https://doi.org/10.22203/eCM.v035a11.

[20] C. Pan, Z. Zhou, X. Yu, Coatings as the useful drug delivery system for the prevention of implant-related infections, J. Orthop. Surg. Res. 13 (2018) 1–11. https://doi.org/10.1186/s13018-018-0930-y.

[21] O. Rzhepishevska, S. Hakobyan, R. Ruhal, J. Gautrot, D. Barbero, M. Ramstedt, The surface charge of anti-bacterial coatings alters motility and biofilm architecture, Biomater. Sci. 1 (2013) 589–602. https://doi.org/10.1039/c3bm00197k.

[22] D. Sun, M. Babar Shahzad, M. Li, G. Wang, D. Xu, Antimicrobial materials with medical applications, Mater. Technol. 30 (2015) B90–B95. https://doi.org/10.1179/1753555714Y.0000000239.

[23] M. Vallet-Regí, D. Lozano, B. González, I. Izquierdo-Barba, Biomaterials against Bone Infection, Adv. Healthc. Mater. 9 (2020). https://doi.org/10.1002/adhm.202000310.

[24] N.A. Khan, M. Durakshan, Cyclodextrin: An overview, Int. J. Bioassays. 2 (2013) 858–865. https://doi.org/10.21746/ijbio.2013.06.003.

[25] Z. Liu, L. Ye, J. Xi, J. Wang, Z. Feng, Progress in Polymer Science Cyclodextrin polymers : Structure , synthesis , and use as drug carriers, Prog. Polym. Sci. 118 (2021) 101408. https://doi.org/10.1016/j.progpolymsci.2021.101408.

[26] P. Jansook, N. Ogawa, T. Loftsson, Cyclodextrins : structure , physicochemical properties and pharmaceutical applications, Int. J. Pharm. 535 (2018) 272–284. https://doi.org/10.1016/j.ijpharm.2017.11.018.

[27] W. Ding, S. Zheng, Y. Qin, F. Yu, J. Bai, W. Cui, Chitosan Grafted With β -Cyclodextrin : Synthesis , Characterization , Antimicrobial Activity , and Role as Absorbefacient and Solubilizer, 6 (2019) 1–14. https://doi.org/10.3389/fchem.2018.00657.

[28] E.P. Goncharova, Y.A. Kostyro, A. V Ivanov, M.A. Zenkova, F. Medicine, RESEARCH ARTICLES A Novel Sulfonated Derivative of β -Cyclodextrin

Effectively Inhibits Influenza A Virus Infection in vitro and in vivo, 11 (2019) 20–30. https://doi.org/10.32607/20758251-2019-11-3-20-30.

[29] S.S. Braga, J.S. Barbosa, N.E. Santos, F. El-Saleh, F.A.A. Paz, Cyclodextrins in antiviral therapeutics and vaccines, Pharmaceutics. 13 (2021). https://doi.org/10.3390/pharmaceutics13030409.

[30] E.M.M. Del Valle, Cyclodextrins and their uses : a review, 39 (2004) 1033–1046. https://doi.org/10.1016/S0032-9592(03)00258-9.

[31] B.G. Poulson, Q.A. Alsulami, A. Sharfalddin, E.F. El Agammy, F. Mouffouk, A.-H. Emwas, L. Jaremko, M. Jaremko, Cyclodextrins: Structural, Chemical, and Physical Properties, and Applications, Polysaccharides. 3 (2021) 1–31. https://doi.org/10.3390/polysaccharides3010001.

[32] Y. Zare, Applied Clay Science Estimation of material and interfacial / interphase properties in clay / polymer nanocomposites by yield strength data, Appl. Clay Sci. 115 (2015) 61–66. https://doi.org/10.1016/j.clay.2015.07.021.

[33] J. Wen, Z. Li, B. Huang, N. Luo, M. Huang, R. Yang, Q. Zhang, X. Zhai, G. Zeng, The complexation of rhizosphere and nonrhizosphere soil organic matter with chromium: Using elemental analysis combined with FTIR spectroscopy, Ecotoxicol. Environ. Saf. 154 (2018) 52–58. https://doi.org/10.1016/j.ecoenv.2018.02.014.

[34] T. Calvo-correas, N. Gabilondo, A. Alonso-varona, T. Palomares, M.A. Corcuera, A. Eceiza, Shape-memory properties of crosslinked biobased polyurethanes, Eur. Polym. J. 78 (2016) 253–263. https://doi.org/10.1016/j.eurpolymj.2016.03.030.

[35] A. Bayu, D. Nandiyanto, R. Oktiani, R. Ragadhita, Indonesian Journal of Science & Technology How to Read and Interpret FTIR Spectroscope of Organic Material, (2019) 97–118.

[36] Correlating mechanical properties of polyurethane-organoclay nanocomposite coatings with processing Anjali Sharma, (n.d.).

[37] Z. Hammoud, N. Khreich, L. Auezova, S. Fourmentin, Cyclodextrin-membrane interaction in drug delivery and membrane structure maintenance, Int. J. Pharm. 564 (2019) 59–76. https://doi.org/10.1016/j.ijpharm.2019.03.063.

[38] M. Špírková, J. Pavličević, Y. Aguilar Costumbre, J. Hodan, M. Urbanová, S.

Krejčíková, Mechanically strong waterborne poly(urethane-urea) films and nanocomposite films, J. Appl. Polym. Sci. 138 (2021). https://doi.org/10.1002/app.50011.

[39] I.S. Stefanović, M. Špírková, S. Ostojić, P. Stefanov, V.B. Pavlović, M. V. Pergal, Montmorillonite/poly(urethane-siloxane) nanocomposites: Morphological, thermal, mechanical and surface properties, Appl. Clay Sci. 149 (2017) 136–146. https://doi.org/10.1016/j.clay.2017.08.021.

[40] G. Verma, Weathering, salt spray corrosion and mar resistance mechanism of clay (nano-platelet) reinforced polyurethane nanocomposite coatings, Prog. Org. Coatings. 129 (2019) 260–270. https://doi.org/10.1016/j.porgcoat.2019.01.028.

[41] P.R. Dandawate, A. Vyas, A. Ahmad, S. Banerjee, J. Deshpande, K.V. Swamy, A. Jamadar, A.C. Dumhe-Klaire, S. Padhye, F.H. Sarkar, Inclusion complex of novel curcumin analogue CDF and β-cyclodextrin (1:2) and its enhanced in vivo anticancer activity against pancreatic cancer, Pharm. Res. 29 (2012) 1775–1786. https://doi.org/10.1007/s11095-012-0700-1.

[42] V. Kakkar, S. Singh, D. Singla, I.P. Kaur, Exploring solid lipid nanoparticles to enhance the oral bioavailability of curcumin, (2011) 495–503. https://doi.org/10.1002/mnfr.201000310.

[43] A. Anitha, V.G. Deepagan, V. V. Divya Rani, D. Menon, S. V. Nair, R. Jayakumar, Preparation, characterization, in vitro drug release and biological studies of curcumin loaded dextran sulphate-chitosan nanoparticles, Carbohydr. Polym. 84 (2011) 1158–1164. https://doi.org/10.1016/j.carbpol.2011.01.005.

[44] C. Wang, Y. Li, G. You, Q. Zhu, The promotional effect of sodium chloride on thermophysical properties of nitrate, IOP Conf. Ser. Mater. Sci. Eng. 772 (2020). https://doi.org/10.1088/1757-899X/772/1/012033.

[45] S.S. Braga, I.S. Gonc, E. Herdtweck, Solid state inclusion compound of S -ibuprofen in b -cyclodextrin : structure and characterisation y, (2003) 597–601. https://doi.org/10.1039/b207272f.

[46] Z. Fallah, Antibacterial and Cytotoxic Effects of Cyclodextrin- Triazole-Titanium Based Nanocomposite, 64 (2021).

[47] M. Babar, A. Sharma, P. Kakkar, A. Arora, T. Arora, Progress in Organic Coatings

Correlating thermal properties of polyurethane / clay nanocomposite coatings with processing, Prog. Org. Coatings. 165 (2022) 106743. https://doi.org/10.1016/j.porgcoat.2022.106743.

[48] M. Jaber, J. Miehe, R. V April, V. Re, M. Recei, V. June, Heavy Metal Retention by Organoclays : Synthesis , Applications , and Retention Mechanism, (2005) 5275–5281. https://doi.org/10.1021/cm050754i.

[49] M.K. Poddar, K. Vishwakarma, V.S. Moholkar, Rheological and mechanical properties of PMMA / organoclay nanocomposites prepared via ultrasound-assisted in-situ emulsion polymerization, 36 (2019) 828–836. https://doi.org/10.1007/s11814-019-0252-8.

[50] J. Chen, X. Qin, S. Zhong, S. Chen, W. Su, Y. Liu, Characterization of curcumin/cyclodextrin polymer inclusion complex and investigation on its antioxidant and antiproliferative activities, Molecules. 23 (2018). https://doi.org/10.3390/molecules23051179.

[51] Z. Yang, H. Peng, W. Wang, T. Liu, Crystallization behavior of poly(ε-caprolactone)/layered double hydroxide nanocomposites, J. Appl. Polym. Sci. 116 (2010) 2658–2667. https://doi.org/10.1002/app.

[52] C. Nanotubes, C. Nanofillers, Polymer Nanocomposites — A Comparison between, (2016) 1–35. https://doi.org/10.3390/ma9040262.

[53] V.A. Online, RSC Advances, (2019) 8326–8332. https://doi.org/10.1039/c9ra00536f.

[54] X. Qiu, Z. Li, X. Li, Z. Zhang, Flame retardant coatings prepared using layer by layer assembly : A review, Chem. Eng. J. 334 (2018) 108–122. https://doi.org/10.1016/j.cej.2017.09.194.

[55] J. Pavličević, M. Špírková, M. Jovičić, O. Bera, R. Poreęba, J. Budinski-Simendić, The structure and thermal properties of novel polyurethane/organoclay nanocomposites obtained by pre-polymerization, Compos. Part B Eng. 45 (2013) 232–238. https://doi.org/10.1016/j.compositesb.2012.09.018.

[56] J.K. Pandey, K. Raghunatha Reddy, A. Pratheep Kumar, R.P. Singh, An overview on the degradability of polymer nanocomposites, Polym. Degrad. Stab. 88 (2005) 234–250. https://doi.org/10.1016/j.polymdegradstab.2004.09.013.

[57] V. Mittal, Polymer Nano - , Micro - & Macrocomposites Series Surface Modifi cation of Nanotube Fillers Characterization Techniques for Nanocomposites Optimization of Polymer Nanocomposite Properties Controlled and Living Polymerizations Miniemulsion Polymerization T, n.d.

[58] M. V. Pergal, J. V. Džunuzović, R. Poręba, S. Ostojić, A. Radulović, M. Špírková, Microstructure and properties of poly(urethane-siloxane)s based on hyperbranched polyester of the fourth pseudo generation, Prog. Org. Coatings. 76 (2013) 743–756. https://doi.org/10.1016/j.porgcoat.2013.01.007.

[59] S. Roy, R. Priyadarshi, P. Ezati, J. Rhim, Curcumin and its uses in active and smart food packaging applications - a comprehensive review, Food Chem. 375 (2022) 131885. https://doi.org/10.1016/j.foodchem.2021.131885.

[60] C. Danel, N. Azaroual, C. Chavaria, P. Odou, B. Martel, C. Vaccher, Comparative study of the complex forming ability and enantioselectivity of cyclodextrin polymers by CE and 1H NMR, Carbohydr. Polym. 92 (2013) 2282–2292. https://doi.org/10.1016/j.carbpol.2012.11.095.

[61] M. Popa, M. Anastasescu, I.C. Gifu, J.M. Calderon Moreno, Hydrophobic Carbonate Coatings on Pure Biodegradable Mg by Immersion in Carbonated Water: Formation Mechanism, Appl. Sci. 12 (2022). https://doi.org/10.3390/app122211674.

[62] Y. Zare, A simple technique for determination of interphase properties in polymer nanocomposites reinforced with spherical nanoparticles, Polymer (Guildf). 72 (2015) 93–97. https://doi.org/10.1016/j.polymer.2015.06.060.

[63] A. Afzal, I. Nawfal, I.M. Mahbubul, S.S. Kumbar, An overview on the effect of ultrasonication duration on different properties of nanofluids, J. Therm. Anal. Calorim. 135 (2019) 393–418. https://doi.org/10.1007/s10973-018-7144-8.

[64] S. Sinha Ray, M. Okamoto, Polymer/layered silicate nanocomposites: a review from preparation to processing, Prog. Polym. Sci. 28 (2003) 1539–1641. https://doi.org/https://doi.org/10.1016/j.progpolymsci.2003.08.002.